Fabrication and Photoelectrochemical Applications of II-VI Semiconductor Nanomaterials

Abhilash Sugunan

Doctoral Thesis

Stockholm 2012

Functional Materials Division

School of Information and Communication Technology

Royal Institute of Technology (KTH), Stockholm

Address

Functional Materials Division

School of ICT

Royal Institute of Technology

Isafjordsgatan 22

SE 164 40, Kista/Stockholm, Sweden

Supervisor

Assoc. Prof. Muhammet S. Toprak

Co-Supervisor

Prof. Mamoun Muhammed

TRITA-ICT/MAP AVH Report 2012:09
ISSN 1653-7610
ISRN KTH/ICT-MAP/AVH-2012:09-SE
ISBN 978-91-7501-382-4

Kista Snabbtryck AB, Stockholm, 2012

Abstract

In this work we investigated fabrication of semiconductor nanomaterials and evaluated their potential for photo-chemical and photovoltaic applications. We investigated different II-VI semiconductor nanomaterial systems; (i) ZnO oriented nanowire arrays non-epitaxially grown from a substrate; and (ii) colloidal CdE (E=Te,Se,S) quantum structures synthesized by solution-based thermal decomposition of organo-metallic precursors.

We have studied the synthesis of vertically aligned ZnO nanowire arrays (NWA), by a wet chemical process on various substrates. We have extended this method wherein nanofibers of poly-L-lactide act as a substrate for the radially oriented growth of ZnO nanowires. By combining the large surface area and the flexibility of the PLLA-ZnO hierarchical nanostructure we have shown the proof-of-principle demonstration of a 'continuous-flow' water treatment system to decompose known organic pollutants in water, as well as render common waterborne bacteria non-viable.

We have studied synthesis of colloidal quantum dots (QD), and show size, morphology and composition tailored nanocrystals for CdE (E=S, Se, Te) compositions. We have studied the influence of crystal growth habits of the nanocrtsyals on the final morphology. Furthermore we have synthesized core-shell, CdSe-CdS QDs with spherical and tetrahedral morphologies by varying the reaction conditions. We show that these core-shell quantum dots show quasi-type II characteristics, and demonstrate with I-V measurements, the spatial localization of the charge carriers in these hetero-nanocrystals. For this purpose, we developed hybrid materials consisting of the core-shell quantum dots with electron acceptors (ZnO nanowires) and hole acceptors (polymeric P3HT nanofibers).

In addition we have also compared the synthesis reaction when carried out with conventional heating and microwave-mediated heating. We find that the reaction is enhanced, and the yield is qualitatively better when using microwave induced heating.

Keywords: ZnO, nanowire arrays, photocatalysis, CdTe, CdSe, CdS, nanotetrapods, nanotetrahedrons, photoconduction, nano-gap electrodes, Type-II QDs, P3HT nanofibers, microwave synthesis.

List of Papers

This thesis is based on the following papers:

1. **A. Sugunan**, H. C. Warad, M. Boman, J. Dutta, “Zinc oxide nanowires in chemical bath on seeded substrates: Role of hexamine”, *J. Sol-Gel Sci. Technol.*, 2006, **39**, 49.
2. **A. Sugunan**, V. K. Guduru, A. Uheida, M. S. Toprak, M. Muhammed, “Radially oriented ZnO nanowires on flexible poly-L-lactide nanofibers for continuous-flow photocatalytic water purification”, *J. Am. Ceram. Soc.*, 2010, **93**, 3740.
3. **A. Sugunan**, S.H.M. Jafri, J. Qin, T. Blom, M. S.Toprak, K. Leifer, M. Muhammed, “Low-temperature synthesis of photoconducting CdTe nanotetrapods”, *J. Mater. Chem.*, 2010, **20**, 1208.
4. R. Afrasiabi, **A. Sugunan**, R. Khan, M. S. Toprak, M. Muhammed, “Microwave mediated synthesis of semiconductor quantum dots”, *Physica Status Solidi (c)*, Accepted, In print, 2012.
5. **A. Sugunan**, Y. Zhao, S. Mitra, L. Dong, S. Li, S. Popov, S. Marcinkevicius, M. S. Toprak, M. Muhammed, “Synthesis of tetrahedral quasi-type-II CdSe-CdS core-shell quantum dots”, *Nanotechnology*, 2011, **22**, 425202.
6. Y. Zhao, **A. Sugunan**, D. B. Rihtnesberg, Q. Wang, M. S. Toprak, M. Muhammed, “Size-tuneable synthesis of photoconducting poly-(3-hexylthiophene) nanofibres and nanocomposites”, *Physica Status Solidi (c)*, Accepted, In print, 2012.

Other work not included in this thesis:

1. X. Wang, Y. Ma, **A. Sugunan**, J. Qin, M. S. Toprak, B. Zhu, M. Muhammed, "Synthesis of uniform quasi-octahedral CeO 2 mesocrystals via a surfactant-free route", *J. Nanopart. Res.*, 2011, **13**, 5879.
2. D. B. Rihtnesberg, S. Almqvist, Q. Wang, **A. Sugunan**, X. Yang, M. S. Toprak, Z. Besharat, M. Göthelid, "ZnO nanorods/nanoflowers and their applications", *Proc.-Int. NanoElectronics Conf.*, 2011, art. no. 5991615.
3. F. Ye, H. Vallhov, J. Qin, E. Daskalaki, **A. Sugunan**, M. S. Toprak, A. Fornara, S. Gabrielsson, A. Scheynius, M. Muhammed, "Synthesis of high aspect ratio gold nanorods and their effects on human antigen presenting dendritic cells", *Int. J. Nanotechnology*, 2011, **8**, 831.
4. Q. Wang, D. B. Rihtnesberg, A. Bergström, S. Almqvist, A. Z. Z. Zhang, W. Kaplan, J. Y. Andersson, **A. Sugunan**, X. Yang, M. S. Toprak, "Compacted nanoscale sensors by merging ZnO nanorods with interdigitated electrodes", *Proc. Int. Soc. Opt. Eng.*, 2011, **8031**, art. no. 80312J.
5. A. Fornara, A. Recalenda, J. Qin, **A. Sugunan**, F. Ye, S. Laurent, R. N. Muller, J. Zou, A. -R. Usama, M. S. Toprak, M. Muhammed, "Polymeric/inorganic multifunctional nanoparticles for simultaneous drug delivery and visualization", *Mater. Res. Soc. Symp. Proc.*, 2010, **1257**, 49.
6. L. Dong, A. Pinos, **A. Sugunan**, S. Li, S. Popov, M. Toprak, A. T. Friberg, M. Muhammed, "Measurement of radiative lifetime in CdSe/CdS core/shell structured quantum dots", *Proc. Asia Communications and Photonics Conference and Exhibition*, 2009, art. no. 5377385.
7. M. S. Toprak, C. Vogt, **A. Sugunan**, "Active cooperative assemblies towards nanocomposites", *Mater. Res. Soc. Symp. Proc.*, 2009, **1140**, 197.
8. **A. Sugunan**, P. Melin, J. Schnürer, J. G. Hilborn, J. Dutta, "Nutrition-driven assembly of colloidal nanoparticles: Growing fungi assemble gold nanoparticles as microwires", *Adv. Mater.* 2007, **19**, 77.
9. **A. Sugunan**, J. Dutta, "Novel synthesis of gold nanoparticles in aqueous media", *Mater. Res. Soc. Symp. Proc.*, 2005, **901**, 257.
10. **A. Sugunan**, C. Thanachayanont, J. Dutta, J. G. Hilborn, "Heavy-metal ion sensors using chitosan-capped gold nanoparticles", *Sci. Technol. Adv. Mater.*, 2005, **6**, 335.

Contributions of the author

Paper 1: Planning of the experiments, performing the experiments, analyzing data, lead in writing the manuscript.

Paper 2: Planning of the major parts of the experiments, performing the experiments pertaining to inorganic material fabrication, analyzing data, lead in writing the manuscript.

Paper 3: Planning of the major parts of the experiments, performing the experiments pertaining to material fabrication, analyzing material characterization data, lead in writing the manuscript. Development and measurements involving nano-gap electrodes was performed by the group of Prof. Klaus Leifer.

Paper 4: Planning of the major parts of the experiments, contributed in analyzing data, contributed in writing the manuscript.

Paper 5: Planning of the major parts of the experiments, performing the experiments pertaining to inorganic material fabrication, analyzing data, lead in writing the manuscript.

Paper 6: Planning of the major parts of the experiments, analyzing data, contributed in writing the manuscript.

List of abbreviations, symbols and non-standard definitions

0D, 1D, 2D, 3D	0, 1, 2, 3 dimensions
Anisotropic	Non-spherical morphologies, usually like rod/wire
Aspect ratio	Ratio of length to width
ATR	Attenuated total reflectance
CdE	Common notation for CdS, CdSe, CdTe
DPA	Diphenylamine
EBL	Electron beam lithography
Exciton Bohr radius	Bohr radius of the excited electron orbital
FIB	Focused ion beam
FTIR	Fourier transform infrared
HMT	Hexamethylenetetramine (hexamine)
HQD	Heterostructured quantum dots
I–V	Current – voltage
Ligand	Molecule that coordinates to the surface atoms
MCP	Monocrotophos
Micelles	Droplets of oil/water suspended in water/oil, stabilized by amphiphillic surfactant molecules
Monomers	Precursor (or its fragment) that will eventually take up a lattice position in the crystal usually after undergoing a chemical reaction in the vicinity of the lattice.
MW	Microwave
Nanogap electrodes	Conducting strip with a nanoscale gap
NTP	Nanotetrapod
Nuclei	Initial cluster of atoms/molecules formed immediately after supersaturation
NWA	Nanowire-array
ODE	1- Octadecene
Optical wavelength	Range of wavelengths of light from ultra-violet to infrared
OFET	Organic field effect transistors
P3HT	poly-(3-hexylthiophene)
Photocatalysis	Catalysis reaction activated by light
PLLA	Poly-L-lactide
Polytypism	Co-existence of two or more stable crystallographic phase
ppm	Parts per million
Precursor	Reactants

PTh	Polythiophene
Quantum dot/wire/well	Materials with three/two/one dimension smaller than its exciton Bohr radius
RF	Radio frequency
RON	Radially oriented nanowiers
Seeds	Small clusters of material onto which further precipitation and/or epitaxial growth is to occur
SEM	Scanning electron microscopy
Surfactant	Molecules that can interface with both oil and water phases due to its amphiphillic structure
TEM	Transmission electron microscopy
TOP, TOPO	Trioctylphosphine, trioctylphosphine oxide
TOP-Te, TOP-Se	Trioctylphosphine-telluride, Trioctylphosphine selenide
[TOP-Te]	Molar concentration of, here of TOP-Te
Twinning	Two separate crystals sharing some of the same crystal lattice points in a symmetrical manner.
UV-Vis	Ultraviolet-visible
$V_{R.M.S.}$	Root mean square value of voltage, R.M.S value is a statistical amplitude of an alternating signal
Wurtzite	A type of hexagonal crystal structure
XRD	X-ray diffraction
Zinc blende	A type of cubic crystal structure
$\theta/2\theta$	Angles of sweep of X-ray detector during XRD measurement.
λ	Wavelength (in this work, unit is nm)
μE	Micro Einstein; number of photons expressed in terms of Avogadro's number

Table of Contents

1. Introduction

In the past decades, nanotechnology has gained prominence in scientific & engineering communities as well as in popular media. Nanomaterials tend to have different physical and chemical properties in comparison to their bulk form, allowing novel and often counter-intuitive applications. Nanotechnology is not a single technology; it is not a jargon for a particular manufacturing process or a particular design for a device. It is instead a broad and interdisciplinary research on fabrication of nanomaterials, tuning their properties and utilizing these novel properties for various applications.

Methods of obtaining nanomaterials vary and mostly depend on the material, its morphology and also the targeted applications. Physical techniques for fabricating nanomaterials including tribology,[1,2] vapor-phase depositions,[3] electric discharges,[4] amongst others. Currently physical techniques are usually limited to specialized vapor deposition techniques for obtaining epitaxial deposition of thin layers[5] and clusters[6] of materials with precision down to atomic layers on various substrates. Other techniques extensively involve solution chemistry and are favored when synthesis of large quantities of nanomaterials at relatively lower costs is required.

Chemical routes for nanomaterials fabrication have matured and there is a very good control over the size,[7] shape[8,9] and most importantly yield when considering a per-batch basis.[10] Applications of nanomaterials cover a wide range of fields including bio-medicine,[11] electronics,[12] optoelectronics,[13] and water purification,[14] amongst many others. Traditionally nanomaterials investigated for (opto/)electronic applications were fabricated by variations of vapor deposition techniques,[15] although recent advances in the chemical routes, allowing synthesis of nanomaterials with good control over its shape (in addition to size) has led to a shift in this trend.[16] This work will be limited to synthesis of group II-VI semiconductor nanomaterials and some applications arising from interactions of its valence electrons with light, with the main focus on the materials chemistry perspectives.

1.1 Overview

This thesis is a continuation and an extended version of a previously published thesis titled ‘Photochemical and photoelectric applications of II-VI semiconductor nanomaterials’, submitted towards partial fulfillment of the requirements for degree of technical licentiate in materials chemistry, in 2010. The focus of this work is to investigate the fabrication of II-VI semiconductor nanomaterials and study the light-matter interaction for potential for photo-electrochemical and photovoltaic applications. We have tailored the charge carrier percolation pathways in nanomaterials with complex

architectures, which consist of rationally designed combination of various semiconductor nanomaterials.

Here we have mainly investigated different semiconductor nanomaterial systems; (i) ZnO oriented nanowire arrays grown on a substrate; and (ii) colloidal CdE (E = Te,Se,S) nanostructures synthesized by solution-based thermal decomposition of organo-metallic precursors. In the case of both these II-VI semiconductor materials, their valence electrons are known to interact with optical wavelength photons.[*] It is also possible to design a complex material system, utilizing the different conduction band minima and valence band maxima of various semiconducting materials to channelize or trap the charge carriers, resulting in interesting potential applications.

The electron-hole pairs generated in ZnO under ultra-violet illumination catalyzes the decomposition of several toxic organic chemicals dissolved in water. This occurs at the surface of ZnO and enhanced surface area of nanorods structures aids this reaction significantly. In this thesis we describe new insights on the mechanisms of formation of ZnO nanostructures (in the form of nanowire-arrays on a substrate) by a solution-chemistry route. Furthermore, we developed a practical route to obtain large quantities of such nanowire arrays on a novel flexible substrate and demonstrate a proof-of-principle of a 'continuous-flow' water purification system.

The light-matter interaction in colloidal CdE quantum dots makes it promising for various photo-electrochemical applications. In this thesis, we have developed a novel low temperature synthesis of CdTe tetrapodal nanocrystals and describe the nanocrystal formation mechanism in our low temperature reactions. We also describe perhaps the first photoconductivity measurements of CdTe NTPs employing 'nano-gap' electrodes of gold. We have also synthesized rationally designed core-shell quantum dots to tailor the spatial distribution of electrons and holes in complex quantum dots. We have also used well known hole conducting and electron conducting materials to demonstrate the tailored spatial distribution of electrons and holes in these complex quantum dots.

Our main motivation is to consolidate the significant recent advances in the multidisciplinary domain of nanotechnology to gain a better understanding of the fabrication processes, development of more efficient fabrication techniques and preliminary assessment of photo-electrochemical applications.

[*] Optical wavelength here refers to the range covering ultraviolet to near infrared (roughly λ = 300–2000 nm)

1.2 Nanoscale effects

This topic is described in greater details in an earlier publication,[17] and is briefly re-described here. In order to explain and bring out various novel phenomena and applications of nanomaterials, or even general chemistry, a proper introduction is justified for the most potent elementary particle in our length/size scales, namely **the electron**.

It is an extreme irony that such a potent elementary particle has been assigned to have a 'negative' charge! As a charged particle, and knowing that there are two equal and opposite kinds of elementary charge, they could have just as well been positive. This 'injustice' was originated by Benjamin Franklin, who arbitrarily assigned the term negative and positive to the property shown by glass and amber respectively to attract small objects when rubbed.[18] It was shown much later that glass lost electrons, while amber gained electrons to become charged and continuing with the naming convention (established for over a century by then), electrons came to possess a 'negative' charge.

Electrons play a central role in many physical phenomena such as electricity, magnetism, thermal conductivity, amongst others. All chemical bonds involve exchange, sharing, or 'loan' of electrons and in some cases the redistribution of electrons within an already bonded molecule causes additional inter/intra-molecular bonds. The strength and nature of these chemical bonds determines most physical and chemical properties of matter, such as melting and boiling points, hardness, conductivity, chemical reactivity, etc. Even the absence of electrons (in a particular energy level/band) is important enough to be assigned a name (holes) and, as will be shown later chapters, play an important role in all contemporary and future 'high-tech' gadgets.

The nature and strengths of the chemical bonds largely determine the properties of matter. Small atoms with few electrons (low atomic number) tend to competitively share or exchange electrons with other atoms to achieve stable octet forming covalent or ionic bonds, respectively. Larger atoms have a lot of electrons, allowing several of such atoms pooling in their electrons to collectively satisfy their stable octet, forming what is called 'free electron gas' model of metallic bonds.

Most solid matter with ionic, covalent or metallic bonding exists with a long range periodic order in the arrangement of the atoms forming crystals.* The exact arrangement, which includes the distances, strength of attachment, and the number of atoms attached to an atom in a particular lattice, determines the many of the physical and chemical properties of the crystalline material.

* The term atom here is usually limited to the nuclei and their inner-shell electrons, while the outer-most electrons actively participate in the various bond formations.

For example in ionic and covalent bonds, the atoms fiercely compete for their electrons and once the bonds are formed, they are rigidly held in place (changing the bond lengths would be difficult without redistribution of the already short supply of electrons). Hence they are usually brittle, have higher melting points, and are nonconductors.* Contrarily, the relatively free electrons in metallic bonds, allow considerable freedom to metallic atoms to change their bond lengths and making metals malleable, have lower melting points and good conductors. The lattice parameters are applicable to a bulk lattice, i.e. for bonds deep with a crystal. At the outermost surface of any crystal, there are atoms which have unsatisfied bonds, and this is compensated within a crystal by strained lattice parameters of the surface atoms with their penultimate atoms. This 'tweaking' usually goes unnoticed in most materials, due to sheer abundance of bulk lattice bonds compared to the strained surface bonds.

If we were to break a chunk of a crystal into two, we increase its exposed surface area, thereby slightly increasing the ratio of strained surface bonds to the bulk bonds. If we keep breaking up this crystal, a time will come when the surface bonds will dominate over the bulk bonds. The particle will have to be very small for this to happen, but it is possible. Theoretical calculations and experiments showed that *this cross-over occurs when dimensions of the matter is hundred nanometers or less.*[19,20] This is the most intuitive 'nano-size' effect: ***dominance of surface atoms***. This concept is schematically shown in **Figure 1**, where the nanocrystal on the right has only the four inner bonds with bulk parameters. The strained bonds of the surface atoms now determine the new properties of the material.[21] The ability to exchange, share, or loan electrons largely determines the chemistry of an atom (or molecule), which in turn is affected by the changes in the lattice bonds in a crystalline material. Hence the properties of a material changes when they are in the form of nanocrystals. Among the several manifestations of the dominance of the strained surface bonds include lower melting points for nanomaterials.[22] The dominance of surface atoms, leads to a heightened chemical reactivity and for this reason, aluminum metal in the form of a fine powder acts as fuel for rocket engines, including the booster stages that were used in space shuttle launches. Part of this work will focus (detailed in chapter 1.8) on a well-known catalytic reaction occurring on the surface of metal oxides (commonly TiO_2 and ZnO) which is known to be very efficient when employing the oxides in the form of nanomaterials.

* Breaking the bonds in an ionic crystal due to melting or dissolution in polar solvents creates mobile ions thereby increasing the electrical conductivity.

Another distinct nano-scale effect is the changes in the quantum mechanical states of the electrons in a nanomaterial. Building up from Bohr's postulate that electrons in an atom can reside only on specific 'allowed' orbits (now known to be orbitals) corresponding to specific energies, this implies that electrons in an atom can absorb or loose discrete quanta of energies to move from its current energy state to the next allowed energy state. For single atoms there are distinct energy states that the electrons can occupy. When millions of atoms come together to form a bulk lattice, due to inter-atomic interactions several closely placed energy states are now available for an excited electron to reside only if the exciting energy is at least enough to reach the lowest of the allowed excited state (this minimum energy is called the band-gap), as shown schematically in **Figure 2**.

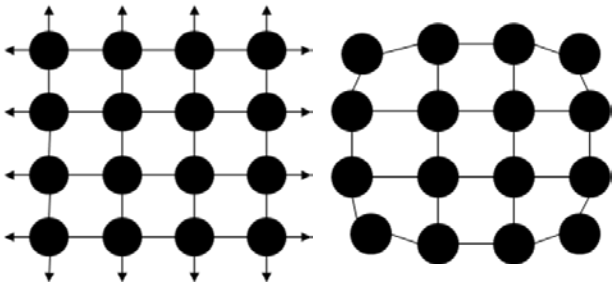

Figure 1. A schematic comparison of lattice of a bulk crystal (left) with a nanocrystals (right).

The availability of allowed states for an excited electron with respect to energy (per unit volume of the material) is called the 'density of states' and for most bulk crystals, there are enough available states to form a continuum called conduction band. The corresponding ground states merge to form the valence band. In other words the density of states is smooth and continuous for bulk crystals.

However when we have a very small crystal (nanocrystal), due to lack of enough atoms, the availability of energy states for electrons become discreet and far apart (**Figure 2**). Such nanocrystals are characterized as atomic clusters and are called quantum confined systems.[23] The requirement for quantum confinement is that the size of the nanocrystals should be smaller than the exciton Bohr radius of the material,[24] which in simple terms is the Bohr radius of the electron residing in the first allowed excited state. This means that an excited electron is physically constrained by the small dimension of the nanocrystal. This spatial confinement can be in only one dimension (1D), two dimensions (2D), or in all the three dimensions (3D). For quantum confined nanocrystals, the band-gap and the density of states becomes sensitively dependant on the size of the nanocrystal (along the confined direction). The

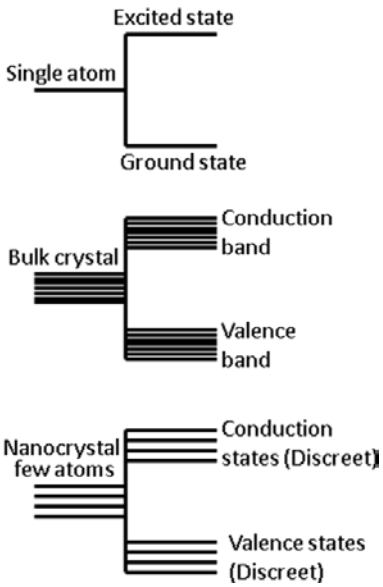

Figure 2. A schematic representation of excited states available to valence electrons in a single atom, atoms in a bulk crystal, and atoms in a nanocrystal.

band gap energy and the separation between available states for an excited electron in a nanocrystal become larger with decreasing size.[23] This is another distinct nano-size effect, wherein, below a certain material dependent critical size, ***the electrons in a nanocrystal becomes 'quantum confined'*** leading to novel size dependent interactions of the valence electrons to specific energies of excitation (notably photons[23] and electric field[25]).

The density of states of quantum confined nanocrystals has characteristic shapes for 2D, 1D and 0D nanomaterials, and the differences are due to the degrees of confinement of the electrons. For 0D nanomaterials, the excited electrons are completely confined in all the three dimensions and they behave analogous to atomic/molecular clusters with discreet states that are well separated in energy. For 1D nanomaterials, the excited electrons experience no confinement along the length of the material, and density of states is quasi-discreet with respect to increasing excitation energy. Finally for 2D nanomaterials, the density of states shows a quasi-continuous step-like increase with increasing excitation energy.[26] These changes in the density of states for excited electrons alters the way excitation energy interacts with the valence electrons, thus changing the fundamental properties with size as well as shape in quantum confined nanomaterials. In the case of larger nanocrystals (not quantum confined), size and shape of the nanocrystals also affects its properties due to differences in surface to volume ratio. For a given mass, 0D nanomaterials have the maximum exposed surface, followed by 1D, and finally 2D nanomaterials have the least.

1.3 Fabrication of nanomaterials

1.3.1 Fabrication of 2D nanomaterials

Fabrication of 2D nanomaterials (including quantum wells) is usually accomplished on a substrate and over the past decades sophisticated techniques have been developed to achieve a controlled deposition down to single atomic layers. Fuelled by the advances in microelectronic fabrication processes, several matured vapor-phase techniques were extended to obtain controlled deposition of 2D nanomaterials.[5] Although vapor-phase techniques are energy intensive and usually require exceptionally clean environments, the technology is mature enough to be commercially viable by large scale production. Indeed multiple quantum well laser diodes are now used in read/write heads for digital optical storage media.[27] Alternative routes to obtain quasi-2D nanomaterials include spin-coating of colloidal nanoparticles or layer-by-layer dip-coating processes (into colloidal suspension of nanoparticles). Both these techniques require synthesis of nanoparticles in colloidal form, by solution chemistry, and the

obtained 2D material is usually textured and non-epitaxial. Such strategies have potential in applications where cost efficiency is more important over high-quality and repeatable performance, such as qualitative sensors.[28] A newly discovered 2D nanomaterial, graphenes (single layer of graphite sheet) can be synthesized by solution-chemistry techniques and are not 'grown' on a substrate.[29]

1.3.2 Fabrication of 1D nanomaterials

One dimensional nanomaterial has nano-scale sizes along two dimensions and having a rod-like or wire-like appearance.* 1D nanomaterials, unlike films and particles, are unique due to the possibility of two axes of alignment with respect to a flat substrate. Planar deposition (parallel to a substrate) of nano-scale wires by extension of various microelectronic fabrication technologies such as chemical etching, [30, 31] electron (or ion) beam lithography [32, 33] has been demonstrated for metallic, or semiconducting materials. These demonstrations are on a small scale.

A number of advanced nano-lithographic techniques notably electron or focused ion beam patterning/writing,[32] X-ray or extreme UV photolithography can be used usually in combination with vapor-phase depositions to obtain nanowire patterns.[34] Typically such nanowires are aligned along the substrates and such techniques are compatible with the planar geometries of contemporary microelectronic devices. These lithography based techniques are usually referred to as 'top-down' approach in nanofabrication (excluding direct writing by focused ion beam).[35]

Another approach called 'bottom-up' involves crystallization of atoms/molecules in a controlled manner (usually diffusion controlled) to obtain size and shape selective fabrication of nanomaterials. In the presence of certain metallic catalysts, vapors of many semiconductor materials crystallize normal to a substrate resulting in vertical, oriented, nanowire-arrays.[34] Several optoelectronic[15] as well as piezoelectric applications [36] have been demonstrated by vertically aligned nanowire arrays of semiconductors that were fabricated by this technique. The commercial potential for these processes are constrained by the need for specialized and expensive substrate for proper oriented growth of the nanowires, and also the complexities and cost of such energy intensive systems and processes.

* A special allotrope of carbon known as carbon nanotubes is an important type of 1D nanomaterial that has not been included in this work since they are fundamentally different from traditional materials in terms of growth mechanism and crystalline microstructure.

An alternative route for 1D nanomaterials synthesis is by solution chemistry, wherein the bottom up approach is achieved by controlled diffusion of ions/atoms (monomers) * in solution to obtain controlled crystallization.[16,37] The advantages of chemical synthesis is the possibility for control of material composition (as alloys and/or heterostructures),[38] fine control of size and shape,[34,39] and most importantly high yield of nanomaterials at relatively lower cost and complexity of processes.[10] Several chemical reactions are now known to produce nano-wires mostly for metallic and semiconducting materials, some of which is described in the next section.

A straightforward method to control the diffusion of precursors to obtain an anisotropic crystal growth is by physical constraint within a solid template. In such a case, crystallization is forced along nano-scale channels that have been previously fabricated within a solid material.[40] This technique works for vapor-phase[41] or crystallization from solution,[42] in fact even molten materials can be frozen into the shape that is complementary to the nano-channel.[43] This technique has been used in combination with electrochemical deposition to obtain several materials including metals, semi-metallic alloys[44] as well as semiconductors.[45] The main disadvantages of this technique includes, poor quality of the obtained crystals (usually polycrystalline),[34] need and complexities of fabricating the template, and commonly encountered need for removing the template after the synthesis of 1D nanomaterial of interest.

Crystal habits of certain materials leads to formation of highly anisotropic crystal structures even in the absence of hard templates. A popular method to fabricate nanowires of noble metals, involves chemical reduction of metal salts with a weak reducing agent, in the presence of amphiphillic surfactant molecules. This technique was referred to earlier as soft-template approach,[34] and it was thought that the surfactant molecules self-assembled in the form of anisotropic micelles within which the reduction reaction of metallic salts took place. Recent studies have shown that differing crystal habits due to specific types of twinning along the fcc [111] planes, leads to various anisotropic morphologies, including nanowires.[46] Such 'template-free' synthesis of 1D nanomaterials usually involves utilizing specific crystal habits to ensure anisotropic crystal growth.[8] This work deals with aqueous synthesis of ZnO nanowire arrays on a substrate and thermal decomposition of organic precursors in non-polar solvents to obtain colloidal quasi-1D nanotetrapods of CdTe. Although the

* In later sections they will be referred to as 'monomers', representing each unit that will eventually take up a lattice position in the crystal usually after undergoing a chemical reaction in the vicinity of the lattice.

exact chemical pathways are different for these syntheses, both techniques utilize the anisotropic crystal habits of hexagonal crystals.

1.3.3 Fabrication of 0D nanomaterials

Since ancient times 0D nanomaterials particularly colloidal gold has been in use for several applications, including coloring agents for stained glass and potteries,[47,48] as well as purported medicinal uses.[49] In the mid-19th century, Michael Faraday performed the first modern scientific experiments with nanomaterials, and determined the particulate nature and size dependent optical properties of colloidal gold.[50] There has been some interest in fabrication of 0D nanomaterials by physical processes like tribology[51] and vapor phase epitaxial depositions[52] followed up by lab-scale proof of principle demonstrations of potential applications.

Due to the extensive knowledge base in chemistry over the past centuries, the field of solution-chemistry based synthesis of 0D nanomaterials is vast and includes size,[7] shape[8,9] and composition controlled synthesis[53,54] of hetero-structured 0D nanomaterials. Notable chemical synthesis techniques for synthesis of 0D nanomaterials include (co-)precipitation,[55,56] sol-gel processes[57,58] and thermal decomposition of organic complexes.[53] The pregnancy test-kits (gold nanoparticles), antibacterial bandages (silver nanoparticles), several formulations of sun-screen lotions (SiO_2 nanoparticles, or other oxide ceramic nanoparticles) are examples of consumer products that involves chemically synthesized 0D nanomaterials.

Some of the techniques for fabrication of 0D nanomaterial can be extended to synthesis of 1D nanomaterial by varying the synthesis conditions.[59] In the next section the thermal decomposition of organic complexes will be described in details as this technique can be used for fabrication of 0D and quasi-1D morphologies of several II-VI semiconductor compositions.

1.3.4 Solution chemistry routes for low dimensional (1D and 0D) nanomaterials

Synthesis of colloidal II–VI semiconductor quantum dots (QDs) by solution chemistry are of significant current interest in materials science, owing to their size and morphology-dependent optical,[60,61,62] optoelectronic,[63,64,65] and photovoltaic properties,[66,67] combined with ease of synthesis and processing. As a result, fabrication of simple morphologies such as spheres and rods has been well established over the last decade.[9,59,39,68]

Thermal decomposition of organic precursors for synthesis of colloidal nanocrystals mainly CdE and ZnE (E=S,Se,Te) composition was pioneered by the Bawendi group.[60] In brief, it involves a rapid

injection of cold trioctylphosphine (TOP) solution containing the metal and chalcogenide precursors into hot (>250 ºC) trioctylphosphine oxide (TOPO) solvent.[60] A rapid nucleation of the CdE nanocrystals is followed by slower growth at a lower temperature. Relatively uniform nanocrystals could be produced by this separation of the nucleation and growth stages in the hot-injection process. In this process, size as well as shape control is primarily achieved by variations in the reaction conditions such as growth time, temperature and monomer concentrations, although choice of precursor complexes are also known to affect the morphology of the obtained nanocrystals. Presently the most common choice of metal precursor is a salt of the metal with fatty acids or alkylphosphonic acids.[39,69]

Colloidal CdTe nanotetrapods by thermal decomposition of organic precursors

Synthesis of colloidal semiconductor nanocrystals with higher complexity, particularly nanotetrapods (NTP), * has attracted recent attention because of their potential in optoelectronic applications. [70] Their unique 3D symmetry allows the possibility of novel alignment of these nanostructures that is difficult to achieve with nanospheres and nanorods.[71] There are several reports in the literature describing the syntheses of structures in the past five years, for several II–VI semiconductor compositions, such as ZnO,[72,73] CdS,[74,75,76] CdTe,[68,77,78] and CdSe.[79,80,81] In most of the reports, the origin of the tetrapodal morphology is ascribed to the polytypism of such semiconductors, exhibiting both cubic (zinc blende) and hexagonal (wurtzite) crystal structures. The cubic (111) face and the hexagonal (001) face terminates with either only anions or cations, and allows for hexagonal arms to grow epitaxially on the four [111] planes of the cubic core.[68,77,82,83] An alternative explanation for the formation of CdTe NTPs is described by Carbone et al.[84] wherein a multiple twinned nucleus with hexagonal structure is shown to 'grow' into a tetrapodal morphology.

From the very first reports of CdTe NTPs, alkylphosphonic acid has been a common choice of ligand for Cd.[77] Recently, Yu *et al.*[83] and Nie *et al.*[85] used fatty acids (oleic acid and myristic acid, respectively) as ligands to obtain CdTe nanocrystals with NTP morphologies. The reaction temperatures chosen in these reports were similar to what is commonly used for syntheses using alkylphosphonic acids as the ligand (typically >250 ºC). Compared to alkylphosphonic acids, fatty

* In this work we describe tetrapodal structures in the context of 1D nanomaterial, owing to their geometry of isotropic attachment of four 1D nanocrystals.

acids bind weakly to Cd, so we envisage a much lower temperature requirement for the synthesis of NTPs by choosing oleic acid as the ligand.

Recently, the use of microwave (MW) irradiation for the synthesis of QDs is gaining popularity due to enhanced reaction rates and yield. There would be more control over the size and optical properties of QDs by dielectric heating since dielectric heating when compared to convective heating, heats the whole volume uniformly and reduces thermal gradient effects.[86] Despite all the reports on synthesis of QDs by MW heating, there are still speculations on whether the reaction proceeds with the same rate with or without the MW-irradiation at the same temperature.[87] The discussions on the reasons for reaction rate enhancements started when some groups observed considerable increase in rate for reactions prepared in MW ovens.[88,89] Thermal and non-thermal effects were claimed to be the reason for the observations. However most of the reports on non-thermal effects were based on comparisons of MW experiments with conventional heating[90] which were not carried out under exact similar conditions. So far no report on the reaction rates and the amount of rate enhancement using MW-assisted synthesis has been published for inorganic nanoparticles.

Colloidal core-shell quantum dots: heterostructured quantum dots

Single crystal QDs degrade over time due to the presence of surface defects and sensitivity to the chemical environment. This can be avoided by synthesizing heterostructures in the form of core-shell nanocrystals.[91,92] Early work on core-shell quantum dots focused on obtaining a thin passivating layer of another semiconductor material with a larger band gap, typically ZnS. This served two purposes, (i) passivation of defects on the core surface and thereby reducing the electron losses, (ii) preventing diffusion of the photoexcited electrons towards the surface of the quantum dot by a potential barrier (due to larger band gap of the shell). As will be described in section 1.4.3, such heterostructured quantum dots are called type-I QDs. Recently other formulations of heterostructured quantum dots (HQDs) have been investigated, among these CdSe-CdS core-shell QDs are promising due to the low lattice mismatch between the core and the shell, allowing for growth of several novel hetero-architectures.

Syntheses of spherical CdSe core coated with a rod like CdS shell have also been reported. It was noticed that in such heterostructures, the CdSe core is located very close to one end of the CdS rod.[93,94,95] Although this asymmetric one-dimensional geometry is very interesting from the materials perspective,[96] the CdS shell covering the CdSe core is very thin except along the long axis of the rod. This could lead to the tunneling of holes into the environment, thereby losing the type-II characteristics.

Another geometry reported in the literature is a CdSe dot embedded within tetrapod CdS nanocrystal.[97] Both these anisotropic geometries are realized due to the intrinsic CdSe and CdS crystal growth modes. It is notable that in both cases, the CdS shell has a hexagonal crystal structure. Depending on whether the CdSe core has a cubic or a hexagonal structure, the final morphology of the heterostructure will be tetrapod or rod-shaped, respectively.[97] Such anisotropic structures are interesting due to their inherent sharp 'tip' and the possibility of aligned deposition on a substrate for optoelectronic applications. Nevertheless, these narrow anisotropic nanocrystals have a limited structural stability and are known to collapse even due to the stress that occurs during the solvent evaporation.[98]

Synthesis of ZnO nanowire-arrays

Several II-VI semiconductors (notably ME; M=Cd, Zn and E=S, Se, Te) are known to be stable with hexagonal crystal structures. These semiconductors are partially polar and in the hexagonal structure (wurtzite), the [001] planes terminate with either cations or anions. Thus the cation terminated ends have a partial positive charge and the anion terminated ends have a partial negative charge, which leads to a high surface energy for the polar plane.[99] Non-polar planes along the side faces are more stable, thus in a thermodynamically stable growth process for hexagonal crystals, large facets are usually the non- polar planes causing an inherently anisotropic growth habit for such crystals.[99] This effect is prominent in ZnO where the hexagonal crystal structure is most common. Utilizing such crystal habit, Vayssieres *et al.*,[100] first reported an aqueous chemical bath process for growth of vertically aligned ZnO nanowire-arrays (NWA) on a substrate. Such NWAs can be grown on a wide variety of substrates. This process involves growth of ZnO rods on various substrates from an 'equimolar' aqueous solution of zinc nitrate and hexamethylenetetramine (HMT) as precursors at temperatures ranging from 55 – 95 ^{o}C.

Lowering the thermodynamic barrier by providing nucleation sites by fixing pre-synthesized ZnO nanoparticles on the substrate (seeding),[101] improves the aspect ratio (ratio of length to width) of the obtained rods,[16] and according to some studies, results in better uniformity.[102] Nucleation sites can be introduced by depositing a layer of ZnO particles by sputtering,[102] or spin coating a layer of colloidal ZnO nanoparticles obtained by chemical route.[16] Alternatively, annealing a layer of zinc foil,[103] or drop-casted ethanol solution of zinc acetate[104] results in a dense layer of ZnO and is known to act as a substrate for growth of ZnO nanowires.

The commonly used precursors for the hydrothermal growth process are zinc nitrate (source of Zn^{2+} ions) and HMT. HMT is a highly water soluble, non-ionic tertiary amine derivative. Variation of the

experimental conditions, such as temperature and the concentration of precursors, allows certain degree of control on the growth rate and the morphology of the obtained nanowires. It was suggested that the main role of hexamine in the growth of ZnO nanostructures in the hydrothermal process is by slowly increasing pH of the chemical bath through decomposition into ammonia.[105]

Since the growth of nano-rods or wires occur epitaxially from the seeds, a pre-decided pattern of nanowires on the substrate can be achieved by patterning the deposition of the ZnO seeds, similar to reports of patterned growth of ZnO rods through the vapor phase route.[106] However, unlike the vapor phase route, the seeded hydrothermal growth can be achieved on a wide variety of substrates and at much lower temperatures.

1.4 Applications of low dimensional semiconductor nanomaterials

Considerable research has been devoted to the fabrication of one-dimensional (1D) nanostructures of various materials due to their unique optical and electronic properties.[34] Here we will focus on applications arising from photon- electron interactions in 1D nanocrystals of ZnO and CdE. The main differences between the two semiconductors are the energy of photons required to excite the electrons. Bulk CdE have band-gaps corresponding to light with near-infrared to blue wavelengths.[78] Thus it will absorb most of the available solar radiation, making them useful in photoelectric applications. Although ZnO is also extensively studied for photovoltaic applications, notably in dye-sensitized solar cells, [107] the role of ZnO is usually limited to aiding the conduction of electrons and not photo-generation of carriers. This is mainly due to the high band-gap of ZnO that limits its interaction to photons with ultra-violet range of wavelengths.

1.4.1 ZnO nanowire arrays

ZnO being a wide band-gap material requires high energy photons (>3.1 eV) to excite the valence electrons, implying that the electron-hole pairs that are generated has similar high energies. This energy is found to be high enough to affect certain bonds in organic chemicals. This photochemical property of ZnO is receiving recent attention due to the severe ecological impact of various industrial and agricultural pollutants in water bodies.[108] The use of metal oxides as photocatalysts for such applications is attractive mainly due to the relatively simple photo-decomposition process and their capacity to convert a large number of organic pollutant molecules into less harmful compounds.[109]

Although TiO_2 (mostly anatase phase) has been extensively studied as effective photocatalyst, recently ZnO has been shown to be more effective than TiO_2.[110, 111, 112] The ZnO-mediated

photocatalysis process under UV and visible light irradiation has been successfully used to decompose organic dye molecules (as a model organic contaminant) for the past few years.[113,114] It is fairly well established that the electron-hole pairs generated in the metal oxide, as a result of photo-excitation, interacts with the solvent to produce chemically reactive free radicals (usually the holes generate $OH^{\bullet}$), [115] which attacks specific bonds of the organic molecule leading to its decomposition.[109] Additives like H_2O_2 and $S_2O_8^{2-}$ is known to enhance the photodecomposition of organic molecules by metal oxides.[109]

Most of the studies on the use of ZnO nanostructures for photocatalytic decomposition of organic molecules involve colloidal nanoparticles. Commercially available TiO_2 (Degussa P25), a widely studied material in the field of photocatalytic reactions, is also in powder form and is used for photocatalytic decomposition by dispersion in water along with the organic contaminant.[116] Although colloidal suspension of nanoparticles has a high surface area, resulting in efficient decomposition of the organic molecule, there is a need for the removal of the metal oxide nanoparticles from the 'slurry', which is time consuming and is usually accomplished by centrifugation.[109] The need for such expensive additional processing step for removal of the active material from the slurry can be avoided by using the powder as nanoparticulate film on a substrate,[117] or arrays of nanowires (NWA) grown on a substrate.[118] For a given area of the substrate, oriented NWA have a higher surface area than a nanoparticulate film.

The freedom in choice of substrate for growing ZnO NWAs by chemical bath deposition was demonstrated recently by Baruah *et al.*[119] by using commercially available non-woven polyethylene microfibers as a substrate material. Another approach to maximize the total surface area of interaction between the photo-active ZnO with the organic molecules was shown by Liu *et al.*[120] wherein nanofibrous mat of ZnO was synthesized by electrospinning polymeric blend containing zinc acetate and cellulose acetate, followed by calcination at high temperatures. These ZnO mat structures have shown to outperform nanoparticulate ZnO in photocatalytic decomposition of organic dye molecules, and this is attributed to the porous nature of the nanofibers. In a similar report, Wang *et al.*[121] described the fabrication of TiO_2 nanofibers by electrospinning and subsequent calcination of an organometallic Ti-precursor followed by growing of ZnO of various morphologies using chemical bath deposition. In both these studies, electrospinning of organometallic precursors and subsequent calcination was used to obtain fibrous metal oxide nanostructures with a high surface area. The final product is a ceramic material which is not flexible. Photocatalytic decomposition of organic molecules is known to occur at

the surface of the metal oxide,[108] however increasing the interactive surface area by fabricating ZnO NWA over a very large area, using brittle or rigid substrates, would make the whole material unwieldy and difficult to immerse into the reservoir of 'contaminated' water.

1.4.2 CdTe nanotetrapods

The relatively low energy level of the photo-generated electron hole pairs of CdTe limits its applicability in photochemistry. Nevertheless they have high mobility[122] and can interact with a wide range of photon energies, suggesting potential in photoelectric and photovoltaic applications.[78] Theoretical studies have shown the suitability of CdTe nanotetrapods as circuit elements.[123] Thus CdTe nanocrystals, especially CdTe NTPs, show good potential as photovoltaic materials. There are several reports in the literature describing the photoconductivity of an ensemble of CdTe nanocrystals either as drop-casted films[124, 125] or embedded within conducting polymers, between transparent electrodes.[126] A more direct evaluation of the optoelectronic properties of this promising nanomaterial is difficult due to its extremely small size. There are a few reports describing the measurement of electrical and mechanical properties of individual CdTe tetrapods and nanorods,[98, 127, 128] although Trudeau et al.[127] also noticed alloying of the electrode metal (Pd) into the CdTe nanocrystal during the deposition causing artefacts in the measurements. However, there is no direct data available in the literature on the optoelectronic properties of individual NTPs. Such evaluations can enhance the understanding of the underlying physics and also help in designing better photoconductor or photovoltaic systems that consists of an ensemble of such nanocrystals.

1.4.3 Core-shell quantum dots

For core-shell QDs, it is possible to engineer the exciton confinement by the choice of the shell material. For applications requiring high efficiency of light emission, the conduction and valence band edges of the shell material should be higher and lower with respect to the band edges of the core material. This will trap both excited electrons and the holes within the core material, allowing a fast and efficient recombination.[129] Such core-shell QDs are called type-I and CdSe QDs coated with ZnS shell are a typical example.[130] For applications requiring long excitonic lifetimes, a staggered alignment of the band edges of the core and shell materials is preferred. In such a structure, photo-excited electrons and holes separate and are located in the different layers of the core-shell QDs.[131] Such QDs are called type-II QDs. Typical examples include CdS-ZnSe[132,133] and ZnTe-ZnSe[134] core-shell QDs.

The case of CdSe-CdS interface is special because, according to the bulk band edge values, both electrons and holes should be confined in the CdSe core, like in type-I QDs. However, optical absorption onset and PL peak wavelength of colloidal CdSe-CdS core-shell QDs show a large red-shift when compared to pure CdSe core QDs.[135] This is a typical characteristic of type-II QDs.[136] The conduction band offset between CdSe and CdS is relatively small compared to the valence band offset,[93,135] with the reported values ranging from +0.2 eV to -0.2 eV.[136] In spite of the uncertainty of the offset value, it is generally assumed that this small offset causes the electron wavefunctions to delocalize over the entire nanocrystal, while the holes remain confined in the CdSe core.[135,137] Thus, the extent of the overlap between the electron and the hole wavefunctions can be tuned by varying the thickness and morphology of the CdS shell. Such 'quasi type-II' QDs show potential applications in optically pumped lasers.[138]

CdSe-CdS core-shell QDs with different shell shapes such as spherical,[94,135,137] rod-like[93,97] or tetrapods[139] have been reported in the literature. One of the earliest studies on CdSe-CdS QDs with very thin spherical shells (up to 3 monolayers; ~1 nm) was reported by Peng et al.[94] The large red-shift in absorption and PL spectrum was attributed to a decrease in the kinetic energy of the electrons due to spreading of its wavefunction into the shell. Spherical CdSe-CdS core-shell QDs with very thick (>6 nm) CdS shell shows reduced blinking as well as suppressed Auger losses, making them attractive for biomedical as well as optoelectronic applications.[135,138]

1.5 Objectives

The main objective in this thesis is to probe the underlying mechanisms involved in the fabrication of selected II-VI semiconductor nanomaterials, and investigate its feasibility in various photoelectrochemical applications. Concisely, the objectives of this thesis are;

1. Study the role of reactant concentrations and temperature during the growth of ZnO nanowire arrays in a chemical bath and obtain a phenomenological explanation of the epitaxial growth process.
2. Fabricate a highly flexible hierarchical nanostructure consisting of nanofibrous mat of poly-L-lactide (PLLA) by electrospinning, with radially oriented nanowires (RON) of ZnO on individual PLLA nanofibers. Such hierarchical nanostructured material retains the flexibility and high surface area of the polymeric nanofibrous mat and has the additional functionality of ZnO nanowires.

3. Develop a simple set up for rapid photocatalytic decomposition of organic contaminants in water in a ‘continuous flow’ mode.
4. Study the synthesis of CdTe nanotetrapods by using less expensive, and benign ligand, namely oleic acid, for Cd, which allows for lowering the temperature requirement for obtaining tetrapodal morphology. Explain the formation mechanism for the tetrapodal morphology.
5. Study the advantages of microwave mediated synthesis of CdSe quantum dots compared with conventional synthesis.
6. Synthesize ‘quasi-type-II’ CdSe-CdS core-shell QDs, and investigate the nature of excited electron and hole distribution within the nanocrystal.
7. Develop the synthesis of a novel ‘giant tetrahedral’ core-shell quantum dots and investigate its formation mechanism
8. Evaluate the photoconduction of CdTe nanocrystals with a ‘nano-gap’ electrode.
9. For heterostructured quantum dots, develop a dedicated electron and hole conducting pathway for potential optoelectronic applications;
    a. For excited electron pathway; study the photoconduction of core-shell QDs conjugated to ZnO nanowires
    b. For the hole pathway; study the fabrication of poly3(hexylthiophene) nanofibers and the conjugation of the core-shell QDs with these polymeric nanofibers. Furthermore investigate the photoconduction of the QD-polymer conjugates.

2. Experimental

2.1 Materials and Synthesis

2.1.1 Aligned nanowire arrays of ZnO

Vertically aligned nanowire array (NWA) of ZnO was prepared by a two-step process consisting of deposition of a uniform and dense layer of ZnO on the desired substrate to act as seeds, followed by subsequent immersion of the substrate into a chemical bath for the growth of NWA of ZnO.

Deposition of seed layer: Two different techniques were used for the deposition of seed layer, depending on the temperature sensitivity of the substrate; (i) for Si or glass substrate, 5 mM ethanol solution of zinc acetate [$Zn(CH_3COO)_2$, Aldrich, 99% purity] was prepared and drop-casted on a clean Si Wafer and heated to 300 °C on a hot plate; (ii) For poly-L-lactide nanofibrous substrates, suspension of homogenous ZnO nanoparticles was prepared based on a method described by Bahnemann *et al*.[140] In brief, it involved preparation of a 1 mM zinc acetate solution in 80 mL of 2-propanol [$(CH_3)_2CHOH$, Aldrich, 99.5% purity] under vigorous stirring at ~50 °C, followed by dilution to a total volume of 920 mL and cooling in an ice bath. To this solution, an 80 mL aliquot of 20 mM sodium hydroxide [NaOH, Merck, 99% purity] solution in 2-propanol was added under continuous stirring and the mixture was immersed in a pre-heated water bath at 50 °C for 2 h. The transparent colloidal solution was stored at room temperature and is stable for months, under ambient conditions.

Growth of ZnO NWA: The coated substrate was placed in an oven at 95 °C for 12 h (or vacuum dried at 60 °C for the same duration for polymeric substrates), for proper fixation. The substrate was then placed in chemical bath containing equimolar solution, with concentrations depending the experiment (20 mM, 1 mM, or 0.5 mM zinc nitrate hexahydrate [$Zn(NO_3)_2 \cdot 6H_2O$, Aldrich, 99% purity] and hexamine [$C_6H_{12}N_4$, Sigma, 99% purity). The growth process was carried out in at various temperatures (60 – 95 °C) for up to 24 h. The growth temperature, time were systematically varied.

Preparation of nanofibrous poly-L-lactide substrates: Poly-L-lactide (Aldrich, Mw = 100000) nanofibers were fabricated by electrospinning technique. The polymer was dissolved in chloroform (7 wt %) and stirred for 2 h. Then it was loaded into a syringe with a stainless steel needle (0.8 mm in diameter) and the needle was connected to the anode of voltage supply (Brandenburg). A collector covered with aluminum foil was connected to the cathode of voltage supply. A voltage of 10 kV was applied between the needle and the collector. The syringe containing the polymer solution was attached to a syringe pump (Cole-Parmer) in a horizontal mount. The distance from the tip of the

needle to the collector is 10 cm and the flow rate is 1 mL/h. The nanofibers were obtained in the form of a non-woven mat with dimensions following that of the aluminum foil cathode (typically 10 × 10 cm).

Synthesis of PLLA-ZnO hierarchical nanostructure: The PLLA nanofibers were immersed for 30 minutes into a colloidal ZnO suspension that was prepared based on a method described by Bahnemann *et al*.[140] and then allowed to dry. This 'seeded' nanofibers was immersed into a mixed aqueous solution of 20 mM each of $Zn(NO_3)_2$ and hexamine and heated to 75 °C for 6 hours. The hierarchical nanostructure consisting of PLLA nanofibers with radially aligned nanowires (RON) of ZnO was washed with de-ionized water and then dried in a vacuum oven for 1 hour.

2.1.2 Colloidal CdTe nanotetrapods

Colloidal CdTe nanotetrapods were fabricated by a hot-injection process that is based on hot injection process for quantum dots, developed by Bawendi and co-workers.[60]

Stock solutions for injections: 0.642 g CdO powder (99.9% Fluka) was added to 13 mL of 1-octadecene (ODE; 90% Aldrich) and 7 mL of oleic acid (90% Aldrich), in a three-necked flask and heated at 160 °C with nitrogen flow for 1 h, to obtain cadmium oleate (Cd-oleate). After cooling down to room temperature the solution was stored in a nitrogen environment. 0.638 g Te powder (100 mesh 99.8% Aldrich) was added to 8.5 mL of trioctylphosphine (TOP; 90% Aldrich) and 11.5 mL of ODE and heated at 200 °C with nitrogen flow for 1 h, to obtain trioctylphosphine telluride (TOP-Te). After cooling down to room temperature the solution was stored in a nitrogen environment. Both stock solutions can be stored for about two weeks, and the container has to be periodically purged with N_2.

Synthesis of CdTe nanotetrapods: In a typical synthesis, 4 mL of ODE was added to a three-necked flask with a magnetic stirrer bar and heated to 180 °C with nitrogen flow. At this temperature, a mixture of 0.4 mL each of Cd-oleate and TOP-Te solutions was quickly injected into the hot solvent. The reaction vessel was immediately taken out of the heating mantle and allowed to cool to room temperature (~10 min). CdTe NTPs were precipitated from the reaction mixture by adding 40 mL of ethanol and collected as sediment after centrifugation. The sediment was re-dispersed in hexane for preparation of transmission electron microscopy (TEM) samples and for ultraviolet–visible (UV–Vis) spectroscopy. Variations from the typical synthesis include different injection temperatures, and cooling sequences.

Synthesis of CdSe nanotetrapods: 4 mL of ODE was added to a three-necked flask with a magnetic stirrer bar and heated to 180 °C with nitrogen flow. At this temperature, a mixture of 1.2 mL of Cd-

oleate solution and 0.4 mL of trioctylphosphine selenide (TOP-Se) was quickly injected into the hot solvent ([Cd]:[Se] = 3:1). The reaction was maintained at this temperature for 5 min and then taken out of the heating mantle and allowed to cool to room temperature (~10 min). CdSe nanocrystals were precipitated from the reaction mixture by adding 40 mL of ethanol and collected as sediment after centrifugation. The sediment was redispersed in hexane for preparation of TEM samples.

2.1.3 Microwave synthesis of CdSe quantum dots

A mixture of 3 mL ODE, 1 mL of 0.5 M Cd-oleate stock solution and 1 mL of 0.5 M TOP-Se stock solution was added to a 2-5 mL MW vial. Ambient air was excluded from the vial and it was filled with nitrogen to avoid any oxidation of the precursors. The sample was heated to 200 °C. The surface temperature of the MW vessel was measured using an infra-red pyrometer. Initiation of the synthesis is carried out at maximum power of 400 W to reach the desired reaction temperature as fast as possible. In order to allow for QD nucleation and growth, the samples were kept for certain preset times at 200 °C. The mixture was then quenched manually by opening the micro-wave cavity and injecting 5 mL oleylamine.

2.1.4 Synthesis of core-shell quantum dots

To grow an inorganic shell of cadmium sulfide (CdS), 1 mL of colloidal CdSe QDs was added into 4 mL of ODE in a three-neck flask. The solution was degassed at 130 ºC for 30 minutes and then heated up to 300 ºC. Cd-Oleate stock solution was injected drop-wise and after 10 minutes TOP-S was injected drop-wise. After 10 minutes waiting time, this process was repeated several times depending on the required shell thickness. The amount of Cd-oleate and TOP-S for the injections was calculated according to the required layer shell thickness. In the case of ZnS shell, the Cd-oleate was replaced by Zn-oleate.

2.1.5 Synthesis of P3HT nanofibers

8 mg P3HT was weighed and added into 2 mL anisole in a dark bottle and the solution was stirred for 10 minutes. Thereafter 2 mL chloroform was added and stirred for 10 minutes. The final solution was put into a dark box for solvent evaporation, under N_2 flow for typically 16 hours. A series of experiments were done with same total concentration (2 mg/mL) using various ratios between anisole and chloroform ranging from 1:1 to 1:4 [mL:mL].

Maintaining the same mixing ratio between anisole and chloroform (1:1), different amounts of P3HT were dissolved to obtain the solutions with different concentrations of 0.1 mg/mL, 0.5 mg/mL, 1

mg/mL and 2 mg/mL. In another experiment, effect of different processing environment was studied. Two P3HT solutions with same total concentration and ratio of solvent were separately put into a dark box with N_2 flow and in a vacuum chamber for 16 h.

2.2 Methods of Characterization

2.2.1 Characterization

Transmission electron microscopy: TEM samples were prepared by drop-casting a dilute suspension of the nanomaterials onto a carbon-coated copper grid and dried in ambient conditions. Typically the dispersion medium was hexane for colloidal NTPs and ethanol for ZnO samples. TEM analysis was done with a JEOL FEG-JEM-2100F operated at 200 kV.

Scanning electron microscopy: SEM imaging was done without any post-fabrication treatment in samples that were grown on Si wafer. For the case of ZnO NWAs grown on glass substrate, to minimize the effect of charging from insulators under the electron beam, the samples were coated with a thin layer of gold by sputtering. The imaging was done using LEO 1550, and Zeiss FEGSEM Ultra 55.

X-ray diffraction: Vertical ZnO NWAs on Si and glass substrates were analyzed with Siemens D5000 X-ray diffractogram (using Cu-kα line) for studying the crystalline microstructure of the ZnO.

Fourier transform infrared spectroscopy: FTIR spectroscopy was performed using a Perkin Elmer Spectrum-One, in the attenuated total reflectance (ATR) mode, by placing a drop of the sample on the crystal window. The consumption of hexamine was monitored by collecting samples for FTIR spectroscopy from a 0.1 M solution of zinc nitrate and hexamine that was placed in an oven at 60 ºC for upto five hours.

UV-Vis spectroscopy: All the spectroscopy analysis was done using Cary 100 Bio UV–Vis spectrometer (dual beam) with a pair of quartz cuvettes as ‘sample’ and ‘reference’. The reference cuvette contained the solvent(s) only and sample contained the analyte in addition to the same solvent(s).

For studying the reaction kinetics, the consumption of TOP-Te (one of the precursors) was followed by spectroscopic methods. Rapid quenching of the reaction (within 2–10 s) was done by quickly injecting a large volume of ODE. To the rapidly quenched reaction mixture, 3 mL of hexane and 20 mL of ethanol was sequentially added and then centrifuged at 10 000 rpm to sediment the nanocrystals. The supernatant was collected and added to a quartz cuvette and its UV-Vis absorption spectrum was

recorded. The absorption at 300 nm was noted and compared with a calibration curve prepared beforehand with known concentrations of TOP-Te.

2.2.2 Continuous flow photocatalytic treatment of aqueous organic molecules

The PLLA-ZnO hierarchical nanostructured material so prepared was inserted into a glass tube. This column was connected to a 50 mL glass bottle (reservoir) and a quartz flow cell, via a peristaltic pump. The flow cell was inserted into a UV-Vis spectrophotometer (Cary 100 Bio), to monitor the changes in absorption spectra in real time. The solution was pumped at a flow rate of 5 mL/minute. Typically, 20 mL water solution of the organic compound (5 ppm) was added to the 'reservoir' and allowed to run through the PLLA-ZnO hierarchical nanostructure for 30 minutes before illumination with a 100 W mercury vapor lamp.

2.2.3 Continuous flow treatment of water contaminated with *Escherichia coli*

A suspension of *E. coli* was added into a diluted nutrient broth solution and 20 mL of this was placed in the reservoir used for photocatalysis, as described above. The solution in the reservoir was flowed through the photocatalytic column for 90 minutes and every 30 minutes, a 1 mL sample was withdrawn from the reservoir, and centrifuged at 2000 rpm. The sediment from the centrifugation was collected and spread on a nutrient agar plate and incubated overnight at 37 °C. The approximate number of viable bacteria was determined by counting the individual colonies visible on the corresponding agar plate after overnight incubation.

2.2.4 Nanogap electrode fabrication

The nanoelectrodes that were used for the photoconductivity measurements were fabricated as described in the literature.[33] In brief, a pattern of 2 μm × 200 nm was made on a Si wafer with a thermally grown 1 μm thick SiO_2 layer by electron beam lithography (EBL) using an FEI XL30 ESEM. After developing the EBL pattern, resistive evaporation was used to deposit a 5–10 nm layer of chromium as an adhesion layer followed by an 80–120 nm layer of gold. Photolithography was then used to pattern 100 μm × 100 μm × 300 nm gold contact pads at the two ends of the line. A gap of 25–30 nm was cut in the EBL line with a focused ion beam (FIB) using Ga^+ ions in a FEI Strata 235 dual-beam FIB at an acceleration voltage of 30 kV. Electrical resistance across the fabricated nanogap electrodes was typically 1000–1500 TΩ. Electrical characterization was carried out in ambient conditions with Agilent B1500A semiconductor parameter analyzer probe station. The probe station

was fixed on a solid table for the mechanic stability of system and placed inside a custom-made thick aluminium box to shield the measurements from external electrical noise and light sources.

2.2.5 Trapping of CdTe nanotetrapods between the nanogap electrodes

The nanogap electrodes were placed in a probe station and 6 μL of diluted colloidal suspension of CdTe NTPs in octane was dropped onto the gap in the electrodes. An alternating voltage of 2.2 V_{RMS} at a frequency of 1 MHz was applied across the nanogap for 60 s and the dielectrophoretic force due to presence of the non-uniform electrical field drew the nanocrystals towards the area of greatest electric field strength. A series resistance of 10 MΩ was used to limit the current flowing through the circuit. After trapping, the liquid drop was evaporated from the substrate using nitrogen flow and the electrodes were rinsed with de-ionized water.

3. Results and discussions

3.1 Aligned ZnO NWAs

3.1.1 Structural characterization

In general, the most commonly observed morphology of ZnO is needle-like or rod-like structures attributed to the inherent anisotropy of the hexagonal lattice with an axial c/a ratio of 1.602.[102] Theoretical calculations predict that the surface energies of the non-polar surfaces of ZnO are small, while the cleavage energy of the polar surface is predicted to be two times larger than the non-polar surfaces.[141] During hydrothermal growth in the presence of ZnO seeds, the highest growth rate is along <002> direction. This form would minimize the total surface energy since the total surface area of the [002] facets would be limited to the tips and hence very low. Nevertheless, it is reported that upon prolonging the growth period, the nanowires grow laterally reducing the overall aspect ratio.[16] In order to achieve a desired aspect ratio, the composition of the chemical bath in which the growth takes place becomes important.*

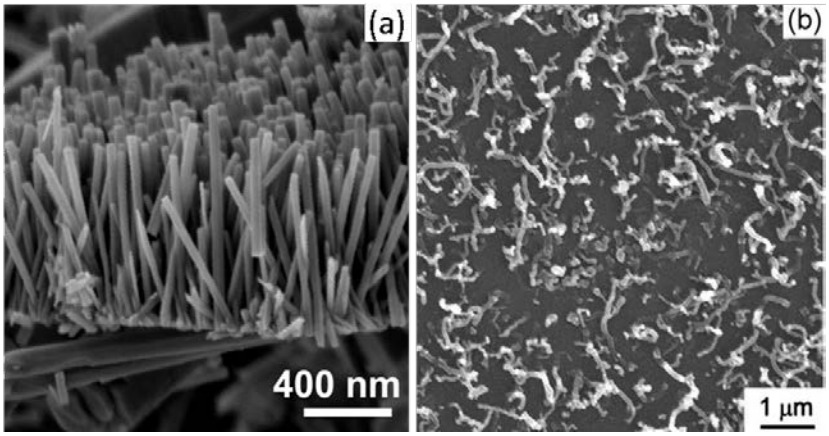

Figure 3. Effect of seed layer density, where **(a)** high density of seeds leads to growth aligned nanowires, compared to **(b)** disperse seeds leading to randomly oriented nanowires.

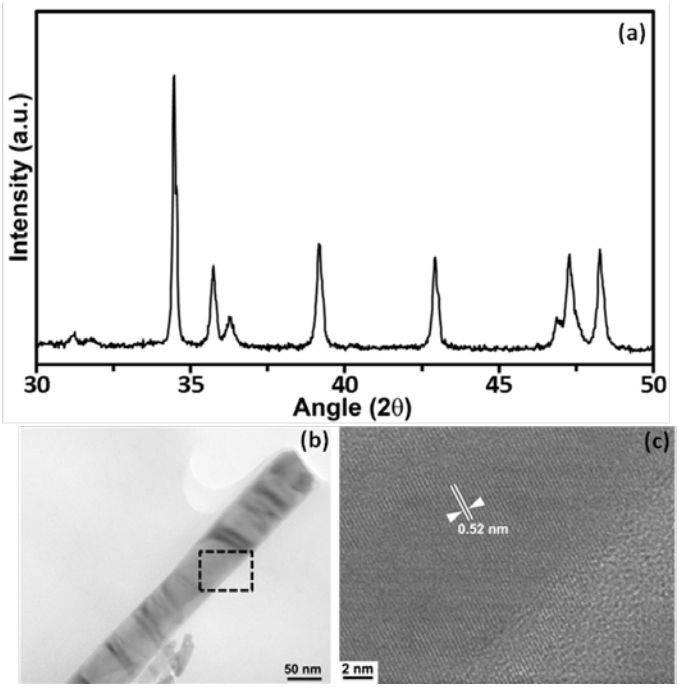

Figure 4. Crystalline nanowires of wurtzite ZnO shown by **(a)** XRD (matching with JCPDS Card: 36-1451), and corroborated with **(b)** TEM and **(c)** HRTEM analysis

* Paper 1

It is reported that a high density of nanowire growth is important to obtain aligned and oriented growth. We tested this by using a diluted suspension of colloidal ZnO nanoparticles for preparing the seed layer on a Si substrate. In another substrate we prepared ZnO seeds by drop casting an ethanol solution of zinc acetate followed by annealing at 300 ºC, which results in a dense layer of ZnO. From **Figure 3a** we can see that using a dense seed layer results in high density of nanowire growth, leading to highly oriented NWAs compared to more or less random growth of ZnO nanowires in the case of substrate with well dispersed seeds (**Figure 3b**).

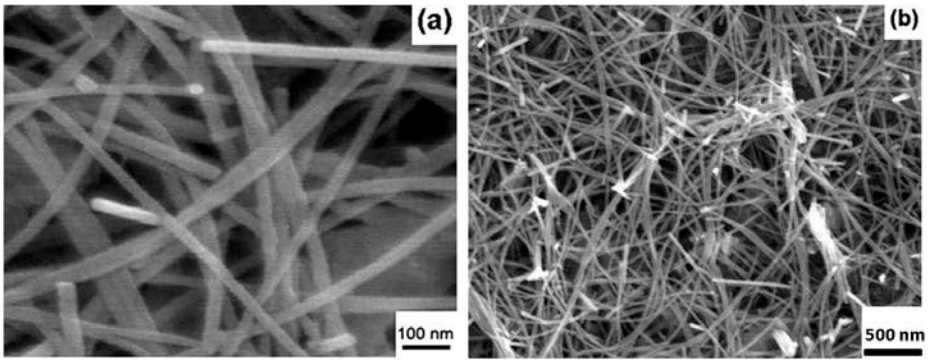

Figure 5. ZnO nanowires after 24 hours of growth **(a)** and **(b)** SEM images at different magnifications.

Due to the aligned orientation of the ZnO NWA, the XRD diffraction pattern obtained from the substrate shown in **Figure 3a** showed a dominance of [002] planes as shown in **Figure 4a**. The XRD pattern matched with hexagonal ZnO crystal structure (JCPDS Card: 36-1451). HRTEM images taken from a single nanowire corroborates the XRD analysis regarding the crystalline nature of the nanowires in the array (**Figure 4c**).*

Extending the growth period to 24 h at 95 ºC typically yielded uniform nanowires of ~30 nm diameter with lengths well exceeding 5 μm, leading to an aspect ratio of over 150 (**Figure. 5**). No significant lateral growth could be observed even after extended periods of growth, though there was evidence of a few nanowires fusing into larger structures, along the non-polar facets. Similar observation of side planes of two or more nanowires fusing to form a single structure with a lower aspect ratio have been reported by others upon prolonging the hydrothermal growth period.[102]

In a phenomenological perspective, ZnO crystal exhibits partial polar characteristics, and in a typical hexagonal structure the (001) plane is the basal polar plane. One end of the basal polar plane terminates with partially positive Zn lattice points and the other end terminates in partially negative oxygen lattice points.[99] It is believed that, in the chemical bath, hexamine being a non-polar chelating

* Paper 2

agent would preferentially attach to the non-polar facets of the nano-wires, thereby exposing only the (002) plane for epitaxial growth. Thus a preferential growth along the <002> direction is made possible.

A recent report shows a reversible reduction of the aspect ratio of ZnO nanorods by introducing acidic anions in the growth medium to cap the polar plane,[101,142] wherein citrate anions probably cap the (001) which terminates with charged $Zn^{\delta+}$. This shows the dependence of the morphology of the ZnO nanowires on the composition of the chemical bath, a clear demonstration of the versatility of the hydrothermal growth process, which can be studied further for controlled nanowire growths.

3.1.2 Hierarchical nanostructures*

Subsequently, we employed flexible nanofibrous mat of poly-L-lactide (PLLA), obtained by electrospinning, as a substrate for deposition of radially oriented nanowires (RON) of ZnO. The dimension of the PLLA nanofibrous mat typically follows the dimension of the cathode plate, and in this work our cathode plate had a dimension of 10 cm × 10 cm.

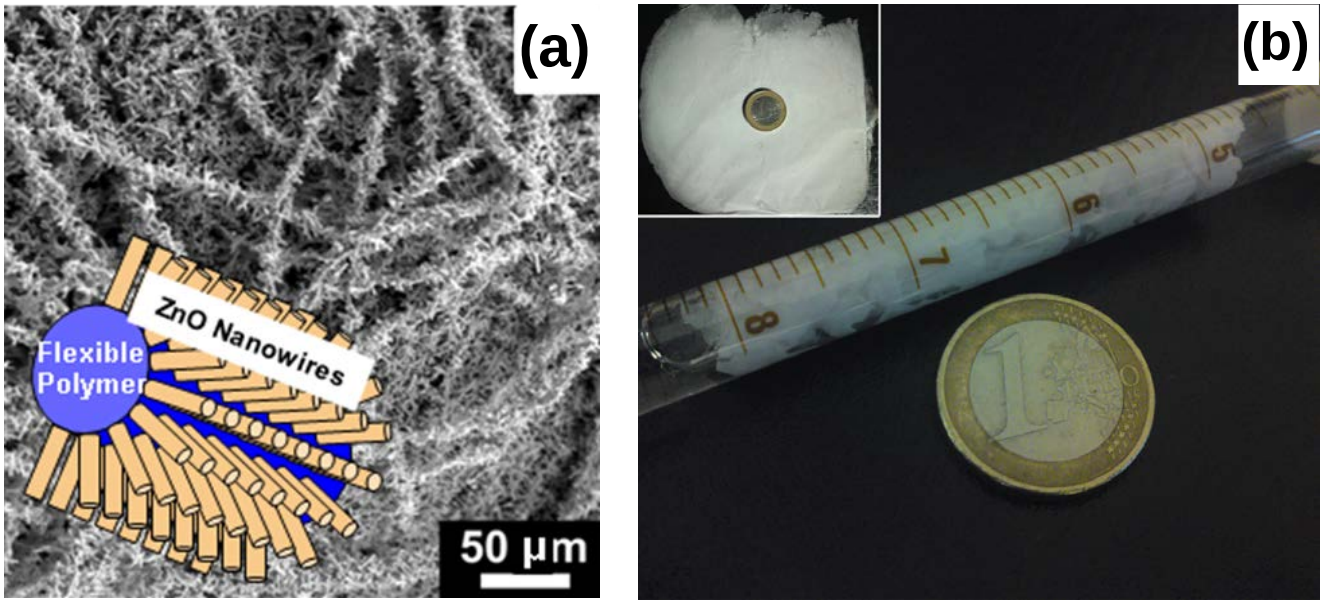

Figure 6. (a) SEM image of the PLLA-ZnO hierarchical nanostructures; **(b)** Optical picture of the Hierarchical nanostructures after insertion into the glass column, A coin (1 €) is placed beside it as a size marker; **Inset** showing the full size of the 'as made' hierarchical nanostructures**.**

Since the polymeric nanofibers cannot be heated above 90 °C we provided the initial nucleation sites for the growth of ZnO nanowires by depositing pre-synthesized colloidal ZnO nanoparticles. The growth of the RON of ZnO was performed under the same conditions as in the case of Si wafer substrate, and the typical growth time was limited to ~6 hours. SEM analysis of the nanofibers after

* Paper 2

ZnO deposition showed a hierarchical 3D nanostructure consisting of polymeric nanofibers which were densely covered by radially oriented ZnO nanowires (**Figure 6a**).

The PLLA-ZnO hierarchical nanostructure was found to retain the high flexibility of the original PLLA nanofibrous mat, and it was possible to insert it into a glass tube (diameter ~1 cm) to form an 'active-filter'. **Figure 6b** shows a photograph of the final material as prepared (**Inset**) and after insertion into the glass tube showing the flexibility and compactness of this polymer fiber-ZnO hierarchical nanostructured material. The significance of the improved flexibility is explained in the next section where we utilize this hierarchical nanostructure for photocatalytic applications.

3.1.3 Photocatalytic Effects

Using the hierarchical nanostructure we then used a 'continuous flow' photocatalysis set up to evaluate the performance in water purification applications. An aqueous solution of organic compounds to be decomposed was passed through the glass tube containing the PLLA-ZnO nanofibers using a peristaltic pump. The glass tube was illuminated by a 100 W mercury vapor lamp (as UV light source) and the photocatalytic decomposition of the organic molecules was monitored by ultraviolet-visible (UV-Vis) spectroscopy (see Experimental Section). For all the experiments, flow rate was maintained at 5 mL per minute, and the reservoir contained 20 mL of aqueous solution of organic molecules. We initially selected methylene blue as the organic molecule to be studied.

When we passed a solution of methylene blue (5 ppm) through the glass tube containing the polymer/ZnO nanostructure we obtained ~90% decomposition within 80 minutes. In order to evaluate the stability of the NWA, we washed the hierarchical nanostructure by passing de-ionized water through the glass tube for 2 hours and then used a fresh solution of methylene blue and performed the experiment again. We repeated this three times, and obtained almost identical decomposition rates for the three cycles. This indicates that the entire PLLA-ZnO hierarchical nanostructure is structurally and chemically stable.

In a following study, we tested the photocatalytic decomposition of two widely used and extremely toxic organic compounds, monocrotophos (MCP; organophosphate insecticide) and diphenylamine (DPA; antioxidant for fruit storage). In one experiment, the reservoir was filled with aqueous solution of MCP (5ppm) and passed through the glass tube containing the hierarchical polymer/ZnO nanostructure under UV-illumination. The UV-absorption spectrum of the solution was recorded every 5 minutes and we observed a rapid decrease in the absorption peak at 215 nm, corresponding to the

photocatalytic decomposition of MCP (**Figure 7a**). We also performed two control experiments (i) with no UV-illumination and (ii) with no RON of ZnO and found negligible decrease in the absorption intensity at 215 nm in both the cases.

In another experiment, to simulate a realistic situation, the 'contaminated' water contained two pollutants (MCP and DPA; 5 ppm each). In this case also, we observed a rapid decrease in absorption peaks at ~200 nm and 232 nm (for DPA) and 215 nm (for MCP) as shown in **Figure 7b**. This demonstrates that simultaneous photocatalytic decomposition of more than one organic contaminant is possible using the hierarchical PLLA/ZnO nanostructures.

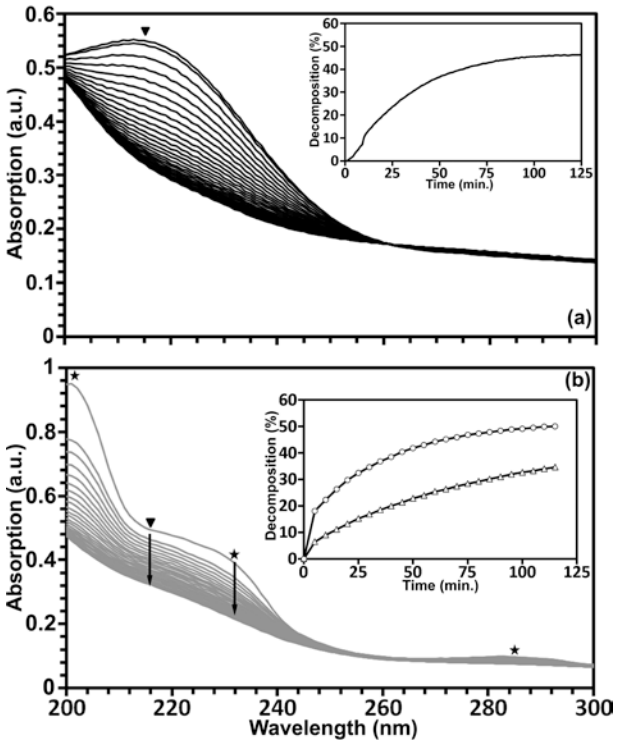

Figure 7. UV absorption spectra of **(a)** aqueous solution of MCP, during continuous flow photocatalytic decomposition. **Inset** shows percent decomposition of peak (marked by ▼) over time. **(b)** mixture of MCP and DPA during photocatalytic decomposition. **Inset** shows the percent decomposition, ○ for MCP and △ for DPA.

Since UV-irradiation is a well-known sterilization technique and furthermore ZnO in the presence of UV light is also known to have enhanced antibacterial effect,[143, 144] we tested the effectiveness of the water treatment system for microbial decontamination of water, by passing an aqueous suspension of *Escherichia coli* through the

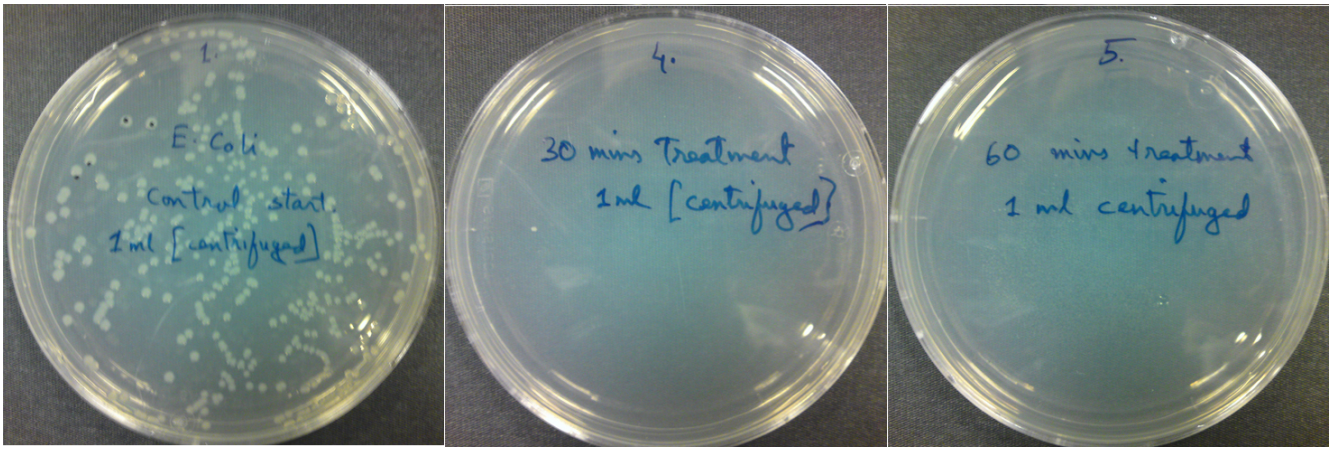

Figure 8. Incubated culture media containing samples after various times of treatment, showing a dramatic decrease in viable bacteria

glass tube containing the hierarchical polymer/ZnO nanostructure under UV-illumination. We passed the 'contaminated' water through the glass tube for 90 minutes and collected 1 mL samples every 30 minutes (see Experimental Section). We found that at the start of the experiment, there were ~325 viable bacteria in the sample. Number of viable bacteria in the sample decreased to 1, 0 and 0 after 30, 60 and 90 minutes of treatment respectively (**Figure 8**). This clearly shows the multi-functionality of our water treatment system with PLLA/ZnO hierarchical nanostructure as the active material, allowing for rapid decontamination of toxic organic contaminants as well as bacteria from 'contaminated' water.[*]

Since the site of photocatalytic decomposition is physically separate from the reservoir containing contaminated/infected water, the need for removal of the photocatalytic material is avoided. Thus the photocatalytic water treatment system described here can be easily modified for point-of-use applications. We are currently investigating the efficiency of photocatalytic decomposition under solar irradiation, which will further enhance the applicability of the material and the system described here. Since the scale up of the fabrication of polymeric nanofibers, as well as the chemical bath deposition of ZnO nanorods is straight forward, larger scale water purification systems with this material is envisaged.

3.2 Colloidal quantum dots of CdE

ZnO almost exclusively exhibits hexagonal crystal structure. However, in case of all CdE (E=S, Se, Te) polytypism is more common, wherein both cubic and hexagonal crystal phase is known to be stable. Unlike the case of crystal growth of ZnO, morphology of CdE nanocrystals also depends on the crystal phase of the seeds (or nuclei in a 'one-pot' synthesis). Growth of nanocrystals is inherently rod-shaped if the seeds have hexagonal crystal structure,[81] and this is similar to the case of ZnO NWAs described in the previous section. However, if the initial nuclei (or seeds) have a cubic crystal structure and if the conditions for growth of seeds favor a hexagonal crystal structure, then the resultant nanocrystals have a novel tetrapodal morphology.[81] The traditional explanation for the origin of tetrapodal morphology is that the four [111] faces (enclosing a tetrahedron) of the cubic crystal terminates with only cations or anions and have very similar lattice parameters, allowing for an epitaxial growth of four wurtzite crystals growing along the <002> directions.[77]

[*] A. Sugunan, A. Uheida, G. K. Rajarao, M. S. Toprak, M. Muhammed, Unpublished results, **2010**.

There are a large number of reports describing isotropic core-shell nanocrystals, wherein irrespective of the crystal structure of the core (seeds) nanocrystal, the shell growth is isotropic resulting in a more-or less spherical final hetero-nanocrystal.[53,54] Importantly, in all those reports the secondary growth of the shell is performed in a deliberately slow and controlled manner, either by slow addition of the precursors for shell growth (drop wise, over a few hours), or in discrete injections to allow for monolayer-by-monolayer growth. If the same amounts of precursor complexes are added suddenly, the shell formation is invariably irregular, and quite often either rod-shaped or tetrapodal.

Another factor favoring anisotropic growth (rod-like or tetrapodal morphologies) in CdE nanocrystals is a fast release of metal and chalcogen monomers from their corresponding complexes during the growth stage of the nuclei,[68,83] and this is important to maintain the growth of the nanocrystals in the diffusion-limited regime.[39] It was also suggested in the early reports of synthesis of tetrapodal nanocrystals that alkylphosphonic acids play an additional role of selective capping of non-polar side plans of the hexagonal crystal.[77] As a result of this, in the reports describing tetrapodal CdE nanocrystals, the most common ligands for the Cd-complex are alkylphosphonic acids, which are known to strongly bind to Cd. Therefore, probably to maintain a fast release (by thermal decomposition) of the monomers, almost all reports describing tetrapodal CdE nanocrystal involves temperatures in the range of 250 ºC or higher.

3.2.1 Effect of temperature*

Since it is known that oleic acid bonds weakly to Cd,[83] when compared to alkylphosphonic acids (a commonly chosen complexing agent for Cd for synthesis of NTPs), we expected a lower reaction temperature would be sufficient to release Cd monomers from the Cd-oleate complex to form anisotropic CdTe nanocrystals. To confirm this, we carried out two syntheses at reaction temperatures of 180 ºC and 250 ºC. To compare the kinetics of the two reactions, we evaluated the temporal decrease in TOP-Te concentration within the first 10 s by UV–Vis spectroscopy. We found

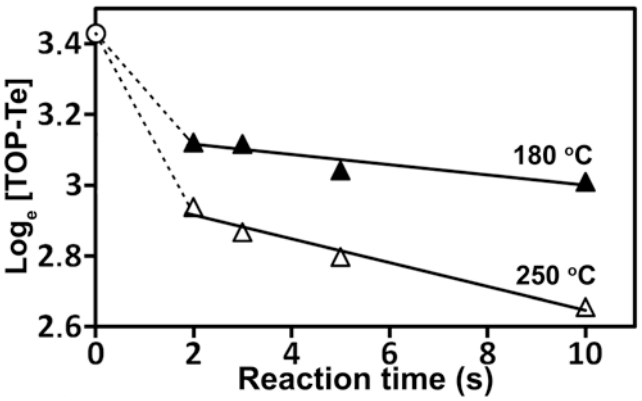

Figure 9 Consumption of TOP-Te; log of the molar concentration of TOP-Te during the first 10 s of the reaction

* Paper 3

that TOP-Te decomposed much faster at 250 ºC and its concentration decreases by ~60% within 10 s, compared to 30% decomposition at 180 ºC for the same time. We found that ln[TOP-Te] decreased linearly with reaction time from 2 to 10 s (**Figure. 9**) confirming that the decomposition of TOP-Te during the growth stage of the nanocrystals for both reaction temperatures is a first order reaction.

We obtained the decomposition rate constant *k* during the growth stage of the nanocrystals for reaction at both the temperatures. It is notable that the intercepts of both curves are much lower than the actual $\ln[\text{TOP-Te}]_0$ because during nucleation, the consumption of TOP-Te is not a first-order reaction. At 250 ºC the calculated rate constant *k* was 0.0336 s^{-1}, and was 2.3 times more than the rate constant at 180 ºC. Thus at 250 ºC, monomers are released rapidly allowing a diffusion-limited growth of nuclei into branched and elongated nanocrystals as described previously in the literature.[39] In the case of the reaction performed at 180 ºC, within the first 10 s only 30% of the TOP-Te is consumed, and the release of Te monomers during the growth stage is also slower. The slow release of monomers will impede the growth of nuclei. It is possible that this slow decomposition of the monomers becomes the rate limiting factor during the growth of the nuclei (reaction limited growth regime[145]) in the reaction carried out at 180 ºC.

3.2.2 Growth mechanism

We then carried out a reaction for longer times at 180 ºC. To monitor the morphology evolution of the nanocrystals, we continued the reaction at 180 (±5) ºC, extracted samples with a syringe after 60 s, 120 s, 300 s, and 600 s and quenched them by adding into hexane (at room temperature). After 600 s we took the reactor out of the heating mantle and allowed the remaining reaction mixture to cool to room temperature for ~10 min. We found very few nanocrystals with NTP morphology in the intermediate samples even after 600 s of continued reaction. The nanocrystals had no defined morphology and the average sizes did not change significantly during this time and were determined to be 5 (± 0.9) nm, 5.2 (±1.2) nm, and 5.2 (±1.0) nm for sample quenched after 120 s, 300 s, and 600 s respectively. However, the sample

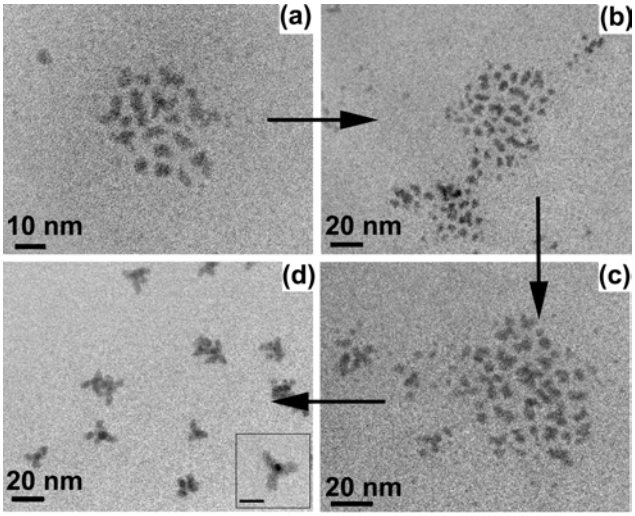

Figure 10. Growth at 180 ºC **(a)**, **(b)** and **(c)** during continued heating there is no tetrapodal nanocrystals present, but **(d)** after slow cooling to room temperature distinctly tetrapodal nanocrystals are obtained.

collected after cooling contained nanocrystals with tetrapodal morphology (**Figure 10**). In another experiment, we took the reactor out of the heating mantle immediately after injection of the precursors. In this case also, we obtained CdTe nanocrystals with tetrapod-like morphology. These observations indicated that the evolution of CdTe nanocrystals into NTP morphology occurred mainly during the cooling. We found no precedent for this observation in the literature, which was presumably because almost all reports of CdE NTPs involve synthesis in a weakly coordinating solvent TOPO (notable exceptions include the work of Yu et al.[83]), and reaction temperatures employed are much higher.

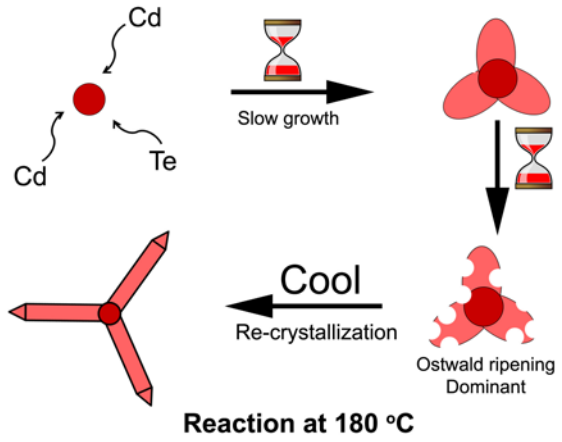

Figure 11. Schematic representation of the proposed growth mechanism at 180 °C

Since the growth of nanocrystals and Ostwald ripening are concurrent processes, when the former is slowed down, the latter emerges. During the growth of the nanocrystals at 180 °C, the slow release of monomers causes Ostwald ripening to overtake the reaction-limited growth of the nanocrystals resulting in more isotropic structures (irregular and more importantly, non-tetrapodal morphologies; **Figure 11**). In this scenario, prolonging the reaction would result in continued re-dissolution of any nanocrystals with complex morphologies and thus explain the near absence of NTPs, and the irregular morphologies of the obtained nanocrystals even after continued reaction for 600 s at 180 °C. On the other hand, cooling down the system lowers the solubility of the dissolved CdTe in the reaction medium leading to fast re-crystallization onto available nanocrystals. This evolution sequence of tetrapodal morphology is unique to our reaction at 180 °C, where the nanocrystal growth rate is limited by the slow release of monomers.

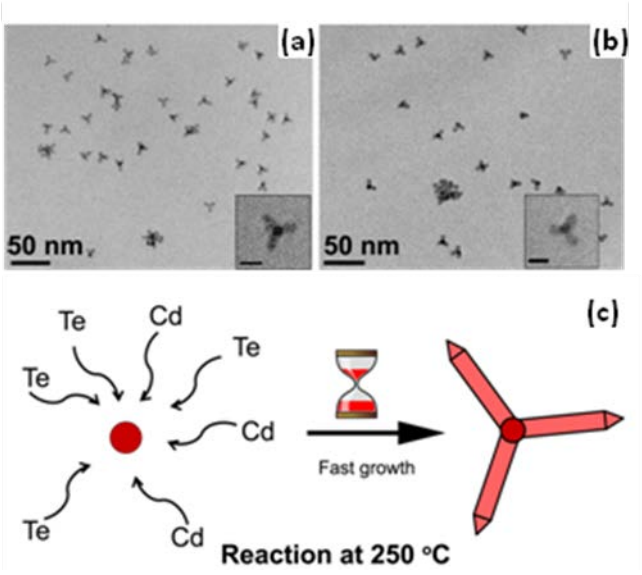

Figure 12. Growth mechanism at 250 °C **(a)** sample taken after 60 s and **(b)** sample taken after 600s showing tetrapodal morphologies. **(c)** schematic representation of the growth at 250 °C

When we performed the same reaction at the

higher temperature of 250 ºC and quenched sample aliquots after 60 s, 300 s, and 600 s after injection of precursors, we obtained colloidal particles with almost exclusively NTP morphology in all the samples (two examples shown in **Figure. 12**). Therefore, at 250 ºC the CdTe nuclei exhibit a diffusion-limited growth regime to grow into NTP morphologies and this is consistent with the conventional understanding of the formation of elongated structures of CdE nanocrystals. This effect is summarized in the schematic shown in **Figure. 12**.

In comparison to other reports in the literature describing the synthesis of CdE NTPs where a combination of an expensive ligand (alkylphosphonic acid) and a weakly coordinating solvent (trioctylphosphine oxide) is consistently used, our reaction medium consists of a relatively inexpensive ligand (oleic acid) and a non-coordinating solvent. Thus, we could reduce the reaction temperature almost by half and still obtain a qualitatively similar final product.

3.2.4 Microwave mediated synthesis*

We compared the synthesis of CdSe QDs by microwave (MW) heating and conventional heating processes. As done with the study of temperature effect, the temporal decrease in concentration of TOP-Se corresponding to different reaction times was studied using UV-Vis spectroscopy. As shown before, and according to a recent study,[146] we assumed that the growth controlled by the rate of precursor decomposition. As shown in **Fig. 13**, the [TOP-Se] continues to decreases rapidly after 50 s of reaction in the case of MW mediated heating, while in the case of conventional heating, the precursor consumption is generally slower and shows indication of saturation after 25 s. The log plot of the precursor concentration in the two reactions follows a linear trend which implies that the reaction is of first order.[69] The reaction rate constants were determined directly from the slopes of the straight lines. We found that for MW synthesis TOP-Se consumption rate k_{mw} (0.0076), which is around double of the value k_{cnv} (0.0042) for conventional synthesis. So we

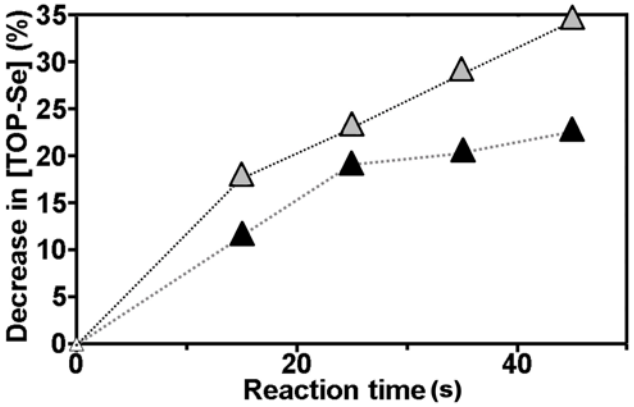

Figure 13. Temporal consumption of TOP-Se in presence of Cd-OA in ODE by MW (Δ) and conventional (▲) heating.

* Paper 4

concluded that the precursor conversion to monomer is enhanced in MW synthesis compared to conventional synthesis.

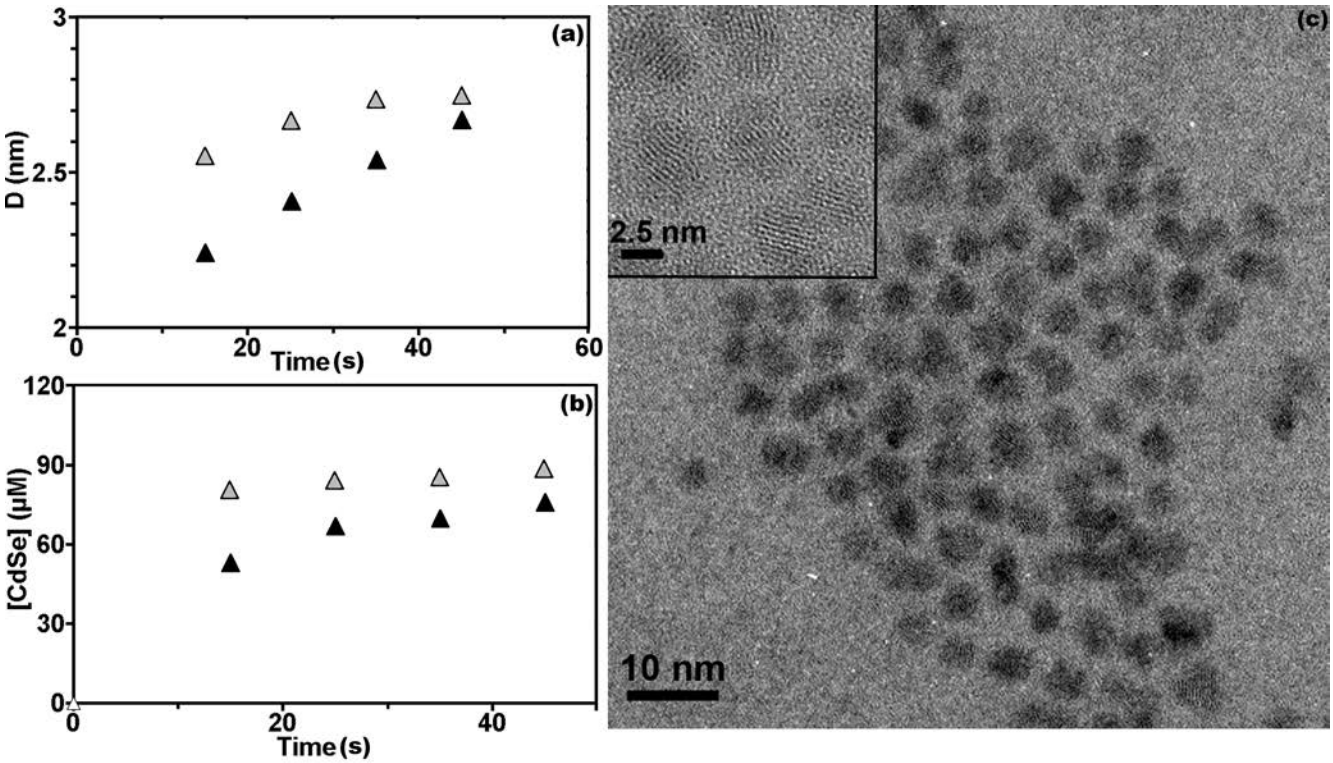

Figure 14. (a) Temporal size evolution of CdSe QDs in MW (Δ) and conventional (▲) synthesis. **(b)** Temporal evolution of CdSe particle concentration for MW (Δ) and conventional (▲) synthesis. **(c)** Typical TEM image of CdSe QDs by MW-assisted synthesis. Inset: High Resolution image of crystalline QDs

We then determined the CdSe QD size and concentration as a function of synthesis time. Both these information can be extracted from UV-Vis spectroscopy.[147,148] The size of the QDs obtained in MW synthesis was larger compared to the conventional synthesis for the same given reaction time and temperature (**Fig 14a**). Due to the enhanced reaction rate in the MW synthesis, we can assume that the nucleation occurred earlier in the MW reaction compared to the conventional reaction. This could explain the reason for obtaining larger QDs. The concentration of the obtained QDs did not vary significantly with time for both the cases. This was expected since the concentration of the nuclei formed in the initial stages of the reaction is not expected to change. The obtained concentration of QDs in the case of MW synthesis was higher showing the MW synthesis is a more efficient process resulting in higher yield, although the conventional reaction allows a better size control, with reaction time. **Fig. 14c** shows a typical TEM image of CdSe QDs by MW-assisted route.

Some early studies speculated that the enhanced reaction rates were the result of MW radiation affecting the orientation and rotation of molecular leading to collisions.[87] Washington et al.[149]

suggested a "selective MW absorption" by the TOP-E precursor as an explanation for the enhanced reaction rates in MW synthesis. We confirmed this by comparing the MW absorption of the precursors relative to the solvent using Beer-Lambert law analogy.[149] Samples containing TOP-Se in ODE, Cd-OA in ODE and only ODE were heated to 230 °C at a constant power of 400 W. Sample containing TOP-Se in ODE reached the designated temperature earliest compared to the other samples, indicating high MW absorption by TOP-Se.

Based on this, we compared the MW absorption of different chalcogenide precursors (TOP-S, TOP-Se and TOP-Te). We found that the MW absorption efficiency was: TOP-Te < TOP-Se < TOP-S. Since the heating is produced by dipolar polarization, difference in electronegativity between the P and the chalcogenide determined the efficiency of energy transfer from electromagnetic energy to heat. We then synthesized CdTe, CdSe, and CdS QDs using microwave synthesis.

3.2.3 Growth of quasi-type II core-shell quantum dots*

Colloidal quantum dots (QD) are attractive in several optoelectronic applications due to their tunable band gap and the possibility to create tailored hetero-structured quantum dots (HQDs) for specific applications. The main motivation for synthesizing HQDs is to control the spatial spread of wave-functions the excited electrons and holes. For instance, most widely studied HQD architecture consists of CdSe-ZnS, core-shell QDs, where the excitons are trapped within the CdSe core to maximize the fluorescence efficiency (type-I HQDs). Such HQDs find widespread applications in bio-diagnostics, light emitting diodes, amongst others.

It was recently shown possible to design a core-shell interface where only excited electron or the hole encounters a potential barrier. Such HQDs are called 'quasi-type-II' QDs. The exciton lifetime in such QDs is very long due to the significantly non-overlapping wave-functions of excited electrons and holes. To obtain such core-shell HQDs, we synthesized QDs with several injection cycles with volumes increasing in square progression. We found that most of the core-shell nanocrystals formed a tetrahedral morphology. The size of final core-shell nanocrystals was 23.1 (± 0.59) nm (**Fig 15a**), showing a significant and uniform shell growth. TEM images of the final CdSe-CdS nanocrystals are shown in **Fig 15a**. Most of the final nanocrystals show a triangular cross section. The variation in contrast within each nanocrystal suggests a 3- dimensional morphology. In addition, we found

* Paper 5

spherical regions with a darker contrast within most of the nanocrystals. These darker central regions could be the CdSe core QDs (**Fig. 15a** inset) and CdSe is known to show a darker contrast in TEM

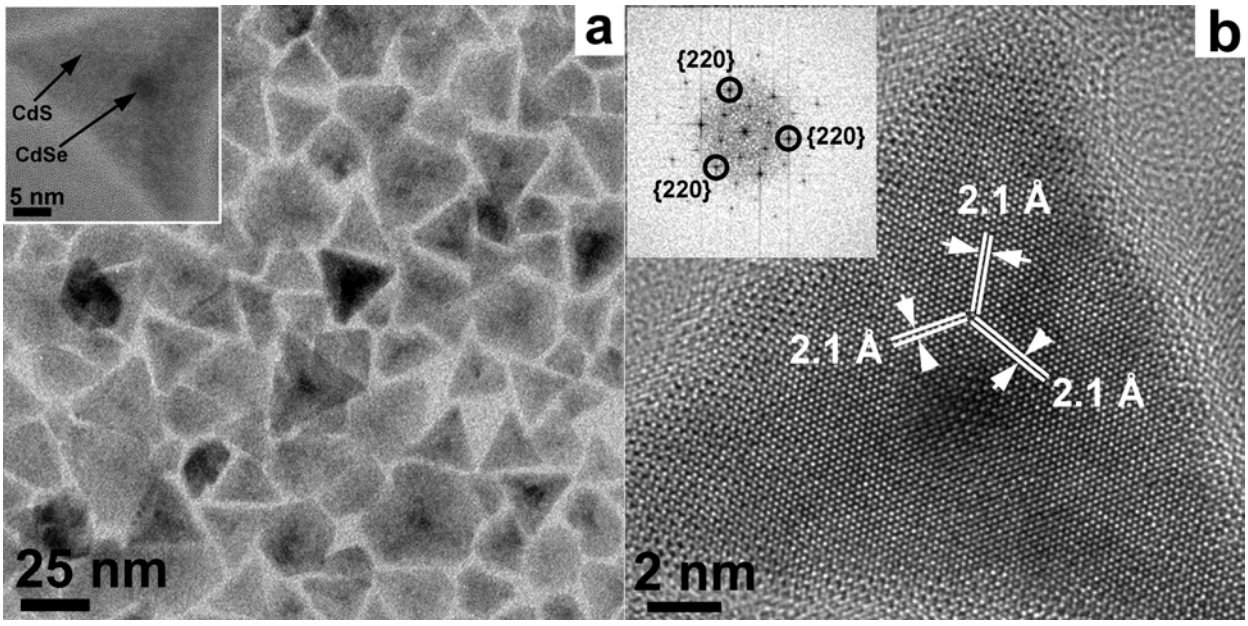

Figure 15. TEM images and analysis of final CdSe-CdS core-shell QDs. **(a)** Representative TEM images of the final core shell QDs (Inset: a single QD showing the central region with dark contrast); **(b)** HRTEM of a single tetrahedral nanocrystal showing the [220] planes of zinc blende CdS (Inset: fast Fourier transform image).

when compared to CdS.[135] We found that the nanocrystal was highly crystalline with well-defined lattice fringes (**Fig. 15b**). Three sets of lattice fringes with 120 ºC mutual rotation could be clearly observed. From fast Fourier transform (FFT) analysis the lattice spacing was found to be 2.1 Å (**Fig 15b,** inset). This matches very well with the d spacing of CdS zinc blende [220] planes, which is 2.06 Å.[150] The occurrence of cross fringes of [220] suggests that the nanocrystal is tetrahedral with four faces of the tetrahedron enclosed by the zinc blende [111] planes. From HRTEM analysis of the CdSe core QDs we found that the most prevalent d spacings were ~0.35 nm and 0.22 nm corresponding to zinc blende (111) and (220) of CdSe.

Since the CdSe core had zinc blende crystal structure the CdS shell also formed zinc blende structure. Thus the final morphology of large core-shell nanocrystal was according to its crystal growth habit along the fastest growing [111] planes. In another experiment we added the precursors for shell growth very slowly (10 mL/h). In this case we obtained core-shell nanocrystals that were more isotropic compared to the nanocrystals obtained with fast injection (30 mL/h) synthesis described earlier. CdE nanocrystals crystallize with a wurtzite structure when the synthesis temperature is relatively high.[77,81] In our case, we obtained a zinc blende structure in spite of carrying out the shell growth at a high temperature of 300 ºC. The reason could be that CdSe core had a zinc blende crystal

structure, so as the layers of CdS shell grew epitaxially; it also had a zinc blende structure. Additionally, alkylphosphonic acid is commonly used as ligand for Cd in anisotropic core-shell CdSe-CdS nanocrystals.[77,139] This ligand is known to promote wurtzite crystal structure. In our case the ligand for Cd was oleic acid. This could be another factor in obtaining zinc blende shell deposition in our experiments.

Thus we find that having wurtzite nuclei which grow with wurtzite structure, we obtain rod shaped nanocrystals. On the other hand, if the cores (nuclei) have zinc blende structure, then the final morphology depends on the crystal structure of the growth stage. If it is wurtzite, then we obtain tetrapodal nanocrystals and if the growth is zinc blende, we obtain tetrahedral nanocrystals. One advantage of tetrahedral morphology is the presence of sharp tips, one of which is always inherently aligned normal to a substrate. Teratpodal morphologies also allow this advantage, but a tetrahedron is more stable and does not break due to capillary forces during solvent evaporation.[98]

3.2.5 Photoconduction measurements of CdTe nanotetrapods*

We also performed preliminary photocurrent measurements of the CdTe NTPs. From a drop of dilute octane suspension, we trapped a few colloidal CdTe NTPs between gold electrodes with a 30 nm 'nanogap' using dielectrophoresis.[33] We then compared the effect of illumination with a 20 W halogen lamp on the *I–V* response of CdTe NTPs.

Figure 16 shows the *I–V* measurements for such a device. From the *I–V* measurements performed under dark conditions we observed current levels in order of 1–2 fA and a non-linear increase in current at voltages >2.5 V, up to a maximum of ~25 fA (**Figure. 16a**). For the same device, in the *I–V* measurements performed under the white light illumination (25 μE $m^{-2}s^{-1}$), the current was significantly higher and was typically in the range of a few pA (**Figure. 16b**). The

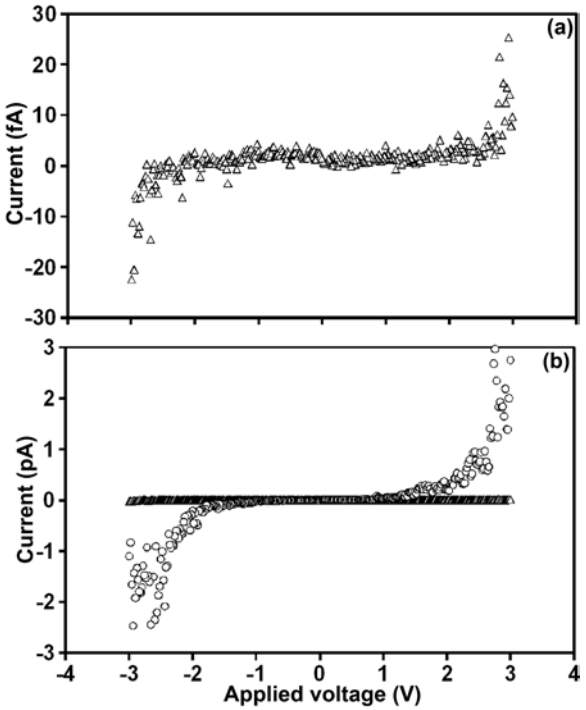

Figure 16. (a) *I–V* response of CdTe NTPs under darkness; **(b)** *I–V* response of CdTe NTPs under illumination (○), the IV response under dark is also plotted as a comparison (Δ).

* Paper 3

current in this case was also non-linear but rapidly increasing even at lower voltages (>1 V). The absorption onset wavelength of bulk CdTe is 820 nm. Though the CdTe NTPs will have a slightly higher bandgap, photons from our white light illumination source had sufficient energy to excite the electrons to the conduction band resulting in enhanced current levels as seen in the *I–V* measurements (**Figure. 16b**). For all devices, the current measured under illumination was enhanced by a factor of 10–300 as compared to the current measured under dark conditions at 2.5 V.

In a control experiment, we performed a similar 'trapping' experiment with a dilute solution of oleic acid and trioctylphosphine in octane and measured its *I–V* response under dark and illuminated conditions. We found no illumination-dependent changes in the current measured across the nanogap. Photoconductivity measurements performed by others on spin-coated thin films of CdTe nanocrystals also show 8–10 times enhancement of current levels under illumination.[125] In another work, Klevkov et al.[151] showed a two-order of magnitude decrease in resistivity of CdTe nanocrystalline films. In both these reports, although a decrease in resistance due to illumination was observed, the measured current levels are much higher compared to our results, due to the larger number of nanocrystals contributing to the conduction.

Recently, Hu et al.[152] employed static electric fields and obtained hundreds of CdSe and CdTe nanorods between 100 nm gap electrodes. In our trapping experiments, the length of the arms of the CdTe NTPs [~15 nm; **Figure. 17 (Inset)**] and the gap between the electrodes (~30 nm) would make it difficult to accommodate such large numbers of NTPs, due to steric considerations. Using SEM imaging we observed some contrast between the nanogap electrodes, which could be attributed to the trapped NTPs (**Figure. 17**). Nevertheless more work is needed to quantify the number and positioning of these NTPs within the nanogap electrodes. From previous trapping experiments on other nanoparticles,[33] we typically observe fewer than 10 nanoparticles between the electrodes under similar trapping conditions. The preliminary optoelectronic measurements reported here are intended only to validate this novel technique, using

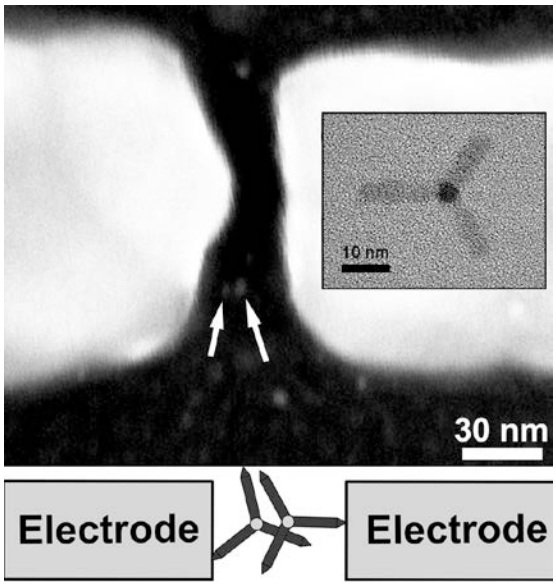

Figure 17. SEM image of the CdTe nanocrystals between the gold Nanogap electrodes. Inset shows TEM image of a single NTP used for the trapping experiments. Below possible schematic arrangement of NTPs between the electrodes.

pre-fabricated nanoelectrodes, for optoelectronic characterization potentially down to the level of single NTPs.

Another reported method for measuring the electronic transport of such nanocrystals involves the thermal deposition of metallic contacts on individual nanocrystals.[127] The method is reported to introduce artefacts into the measurements due to diffusion of the metal into the CdTe nanocrystal.[127] This makes our 'direct and artefact-free' evaluation of the photoelectric properties of CdTe NTPs described here unique and significant, particularly since CdTe nanocrystals are widely reported to be active materials in future photoconductors and solar cells. We are currently performing a thorough investigation of the photoelectric properties with respect to different morphologies and material architectures, which will be described in detail elsewhere.

3.2.6 Tailoring the energy levels*

Unlike simple quantum dots of CdSe and CdTe described in the above sections, the core-shell CdSe-CdS quantum dots are so-called 'quasi-type II'. In order to confirm the nature of the charge carrier separation we performed a series of optical experiments.

Table 1. List of core-shell geometries studied for optical characterization

		Absorption onset	Decay time τ_1	Decay time τ_2
Core CdSe; 2.2 nm		489 nm		
	Shell CdS; 1nm (CS1)	548 nm	0.5 ns	7.3 ns
	Shell CdS; 2 nm (CS2)	569 nm	0.4 ns	8.5 ns
Core CdSe; 2.8 nm		536 nm		
	Shell CdS; 1nm (CS3)	588 nm	0.4 ns	9.2 ns
	Shell CdS; 2 nm (CS4)	604 nm	0.4 ns	6.2 ns
	Shell ZnS; 1 nm (CS-Ref)	560 nm	0.08 ns	2.7 ns
Core CdSe; 3.9 nm		577 nm		
	Shell CdS; 1nm (CS5)	620 nm		
	Shell CdS; 6 nm (CS6)	621 nm		

The CdSe core QDs were synthesized of three different diameters and coated with spherical CdS shells of various thicknesses (**Table 1**). When compared to CdSe core QDs, the core-shell QDs for all shell thickness showed significant red-shift in the band-edge absorption (**Figure 18a–c**). In the absorption spectra of core-shell QDs coated with 1 nm CdS layer (CS1, CS3, CS5; see Table 1), the extent of the red-shift was larger for smaller core diameters, namely 59 nm (0.27 eV), 52 nm (0.20 eV), 43 nm (0.15 eV) for the 2.2 nm, 2.8 nm and 3.9 nm diameter cores, respectively. The red-shift observed with increase of the core size for the same shell thickness occurs because of the size

* Paper 5

dependence of the electron and hole energy levels in the QD core. The lattice mismatch between the core and shell is known to cause a strain-induced shift in the absorption spectrum of colloidal core-shell QDs.[150] However the lattice mismatch between CdSe and CdS is 3.9% and 3.7% for hexagonal and cubic crystal structures, which is very low and is not expected to cause any significant red-shifts in absorption spectrum.[135]

The different behavior for small and large core diameter QDs can be understood as follows: In quasi-type II core-shell QDs, absorption at the band gap primarily takes place in the core, because the spatially direct transitions in the core have a larger transition matrix element than the spatially indirect core-shell transitions. This claim is supported by the spectral shape of the ground state absorption peak for the core-shell QDs, which is very similar to the shape of the pure core QDs. This peculiarity is specific to the CdSe-CdS QDs with a small conduction band offset. In type-II QDs with a large band offset, e.g. ZnSe-CdS QDs, the spatially indirect transitions are prevailing for large shell thicknesses and the ground state absorption peak is strongly broadened with a long red tail.[150] Nevertheless, in our CdSe-CdS QDs the spatially indirect transitions in absorption do occur, and their relative weight is larger for the small core diameters compared to the large ones, simply because of the larger amount of the core material in the larger core dots. The absorption spectra would then be a mixture of the spatially direct and indirect transitions.

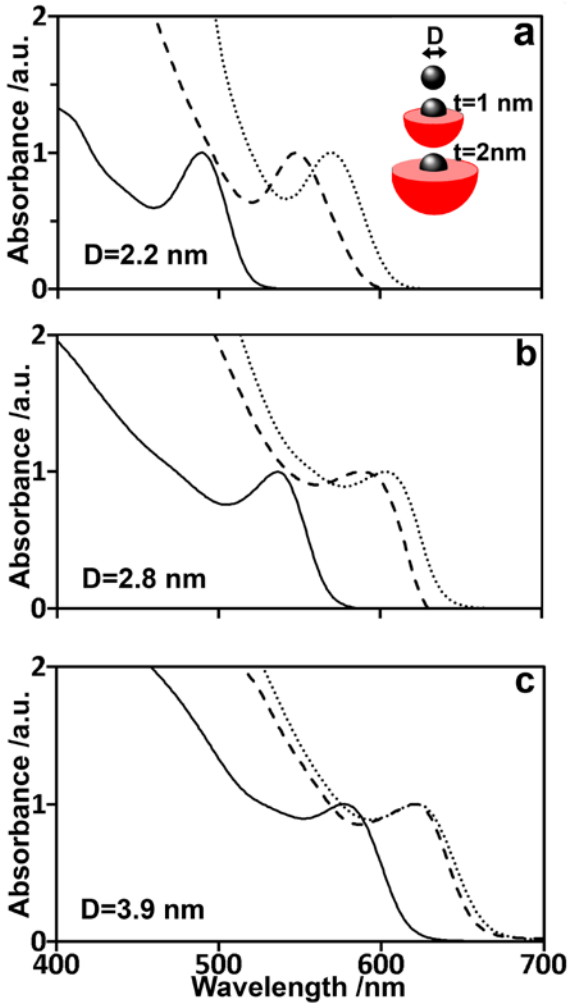

Figure 18. (a–c) absorption spectra of CdSe core QDs (solid line), compared to the absorption of core-shell QDs with 1 nm CdS shell (dashed lines) and 2 nm CdS shell (dotted line; in trace c dotted line shows 6 nm shell); **(d)** Schematic representation of the core-shell geometries.

This observation is clarified in **Figure 19a**, where large CdSe core (3.9 nm) is coated with various shell thicknesses and still there is negligible redshift in the absorption band edge of the absorption spectrum of the core-shell QD, due to dominance of spatially direct transitions. In comparison, the PL peak wavelength shows a noticeable red-shift with increasing shell thickness for all core diameters (for

the 3.9 nm core, see **Figure 19b**). Luminescence, contrary to absorption (provided that the electron transfer from the core to the shell states is much faster than the recombination time) is spatially indirect. This is the main reason for the Stokes shift between the absorption and the emission spectra. The Stokes shift increases with the increased shell thickness because in thicker shells the quantum states have lower energies.[153] The Stokes shift dependence on the shell thickness as well as the above-discussed peculiarities of the absorption spectra confirm the type-II character of the CdSe-CdS QDs

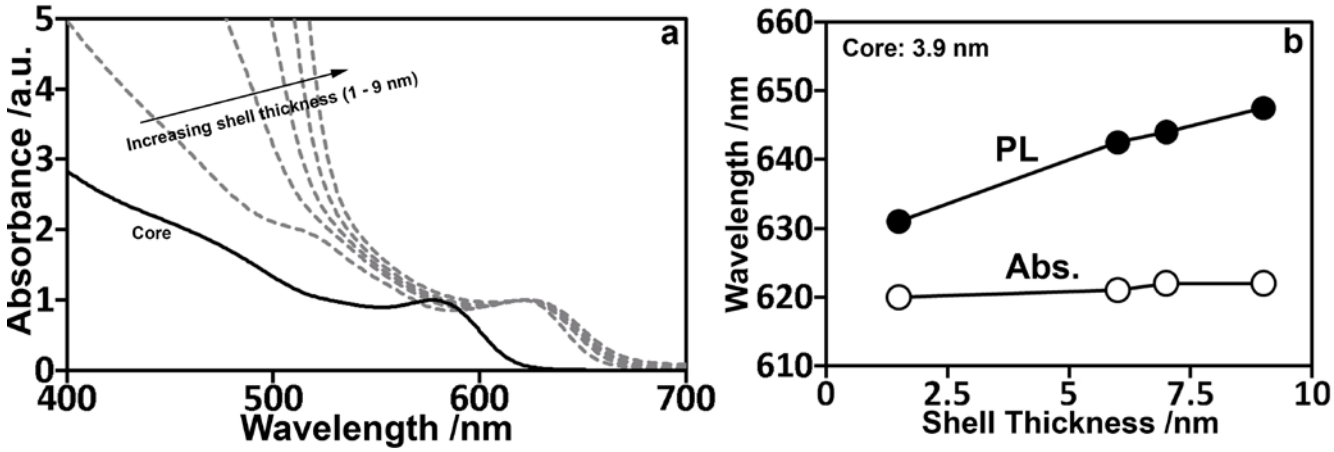

Figure 19. (a) Absorption spectra of core-shell QDs with varying CdS shell thickness (1–9 nm; gray dashed lines) with the 3.9 nm CdSe core (solid black line); **(b)** Red-shifts in absorption spectra as a function of the shell thickness of CdSe-CdS core-shell QDs compared to the shifts of the emission peak.

and clearly shows that the ground energy level in the CdS shell conduction band is below the level of the conduction band of the CdSe core.

The measurements of the PL dynamics show that the PL decay has double-exponential shape with characteristic times τ_1 and τ_2 (**Table 1**). The exciton lifetime is affected by the spatial separation of the electron and hole.[139] The exciton lifetimes in studied quasi-type-II CdSe-CdS QDs for all core and shell sizes were much longer compared to the reference type-I QDs (CS-Ref). It is notable that samples CS3 and CS-Ref have identical core and shell parameters except for the shell material, or, in other words, the alignment of shell energy levels compared to CdSe core. Hence the 3 times increase in exciton lifetime between CS3 and CS-Ref can be attributed to the reduced overlap of the electron and hole wave-functions in the CdSe-CdS QDs.

Although these results indicate spatial separation of excitons, specifically identifying whether electrons, holes or both are being confined across the core-shell interface is difficult. In order to directly determine whether the holes that are confined within the CdSe core, while the electrons are delocalized throughout the entire nanocrystal, we fabricated two separate composite materials for probing the hole conduction pathway and the electron conduction pathways.

3.2.7 Pathway for holes*

For hole conducting material, we investigated semiconducting polymers. Polythiophene (PTh) and its derivatives such as poly-(3-hexylthiophene) (P3HT), are usually preferred due to their far greater solubility in common solvents and less sensitivity to oxygen.[154] P3HT is a 'hole conductor' with the highest reported conductivity so far,[155] and has been extensively used in organic field effect transistors (OFETs),[156] solar cells,[66] amongst others. It was observed that the field-effect mobility of OFETs was dramatically improved when P3HT was in the form of nanofibres.[157]

It was subsequently found that due to strong π–π interactions the crystal growth habit of P3HT favored formation of anisotropic wire-like morphology. In such crystalline form, conduction occurs along the π-π stacking direction.[158] Xu et al. showed that the crystalline P3HT nanofibres have a higher conductivity compared to P3HT film, due to the regular and dense arrangement of the monomer molecules.[159]

We modified the common 'whisker method' and developed a simple and reproducible way to obtain P3HT nanofibres with controllable size. By mixing a poor solvent (anisole/p-xylene)[158] and a good solvent (chloroform) at various ratios, P3HT can be dissolved at room temperature. The gradual evaporation of chloroform decreases the solubility of P3HT in the mixed solvents, resulting in precipitation of P3HT nanofibres.

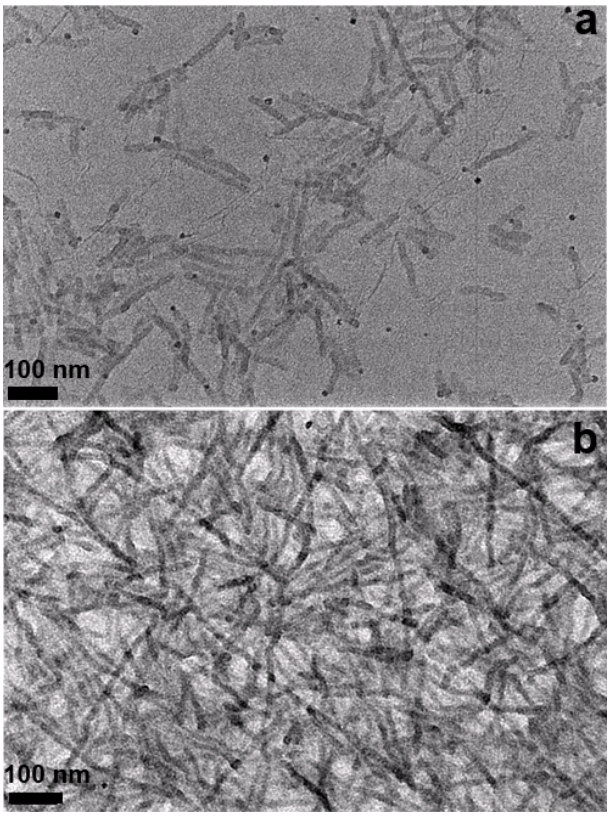

Figure 20. Transmission electrons microscope (TEM) images of P3HT nanofibres obtained with different total concentrations while maintaining the same ratio of solvents at 1:1. **(a)** 0.1mg/ml; **(b)** 2mg/ml

From several TEM images of the nanofibres, we calculated the average diameters. When the ratio between anisole and chloroform was 1:1, the average diameter of obtained P3HT nanofibres was 16 nm (±1.6 nm). Meanwhile, the average diameter of nanofibres obtained by using a solvent ratio of 1:4 was 20 nm (±1.6 nm). These measurements show

* Paper 6

that the ratio between solvents influences the diameter of P3HT nanofibres. This was expected since abundance of chloroform (good solvent) in the initial solution allowed formation of wider lamellae with more P3HT chains assembling in each layer. Subsequent evaporation of chloroform increases the concentration of the P3HT solution beyond the supersaturation resulting in crystallization by stacking of the lamellae via π-π interaction, as described in the literature.[158]

Another series of experiments was done to find the effect of total concentration of P3HT in the mixed solvent. Ratio between anisole and chloroform was maintained as 1:1 for all these samples. It was found that the P3HT nanofibres were progressively longer in with increasing total concentration of P3HT. During the precipitation, larger amount of P3HT was helpful to grow longer nanofibres. However, all the P3HT nanofibres have similar average diameters of ~16 nm. This further confirmed that the diameter of the nanofibres is largely determined by the ratio of the solvents, while the total concentration of solution only affected the length of nanofibres. **Figure 20** shows two example TEM images of the nanofibers obtained with the lowest (0.1 mg/ml) and highest (2 mg/ml) concentration.

Having developed hole conducting polymer nanofibers, we combined them with the quasi-type II core-shell QDs . This was done by adding the colloidal quantum dots into a suspension of the polymer nanofibers in cyclohexane and stirring for 48 hours. We speculate that the thiophene moiety can conjugate with the Cd and aiding in the assembly of the QDs along the nanofibers. A schematic representation of the relative band level alignments of this nanocomposite is shown in F**igure 21a**.

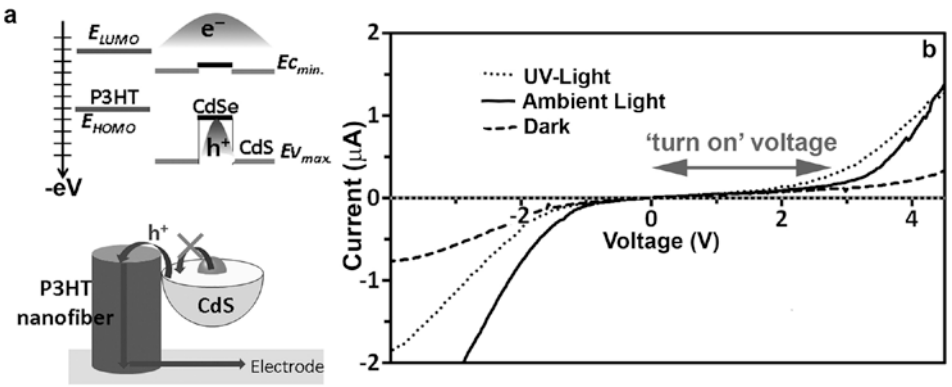

Figure 21 (a) schematic representation of the band levels and hole pathway; **(b)** Typical IV response of the P3HT-HQD nanocomposite.

The nanocomposite solution was drop-casted on a gold finger electrode with a spacing of 3 μm between the fingers. We compared the I-V response across the electrodes, under no illumination, white light illumination (0.1 mW/cm^2) and under UV illumination (360 nm; 0.5 mW/cm^2). The measured I-V response is shown in **Figure 21b**. The current response under all the three illumination conditions shows a distinct 'turn-on' behavior. Interestingly, the 'turn-on' voltage decreases with the energy of the illuminating light, lowest under UV illumination, and highest under dark conditions. Nevertheless,

these I-V curves suggest that until a sufficient threshold voltage is provided, there is negligible current flow. Recalling that P3HT is a hole-conductor polymer, this I-V response shows that under low bias voltage very few holes from the HQDs reach the polymeric nanofibers. Under sufficiently high bias voltage the holes can overcome the potential barrier at the core-shell interface and reach the shell and eventually the P3HT nanofibers, resulting in a sharp increase in measured current. For comparison we performed similar I-V measurements on pristine P3HT nanofibers. In this reference cases we did not observe a similar 'turn-on' voltage requirement. For pristine P3HT nanofibers, visible light illumination resulted in the highest current, while in the case of nanocomposite with CdS QDs UV illumination resulted in the highest measured current levels. Both these observations are consistent with the absorption spectra of the corresponding samples. For the *I-V* response measurements we used HQDs with very thick CdS shell in order to prevent any chances of tunneling of the spatially confined charge carriers (holes) through a thin shell. A more detailed study comparing the 'turn-on' voltages with respect to various shell thickness may help clarify the physics of hole injection from HQDs into the P3HT nanofibers.

3.2.8 Pathway for electrons*

To estimate the availability of the excited electrons on the surface of the HQD nanocrystals, we combined these HQDs with ZnO nanowires, by dip-coating (**Figure 22**) and then measured the *I-V* response using similar electrodes and conditions as described above.

In the case of HQDs combined with ZnO nanowires, the current levels show an increase with voltage even at low voltages and we could not observe any noticeable 'turn-on' behavior in the current response curve (**Figure 22c**). Since ZnO has a band gap energy corresponding to that of UV light, we expect that under visible light illumination the charge carriers originate from the HQDs and are injected into the ZnO nanowires. Since ZnO is a well-known as electron acceptor due to the favorable alignment of conduction band levels between the CdS and ZnO (**Figure 22c inset**), the absence of a 'turn-on' voltage indicates that the excited electrons generated within the HQDs are freely available at the surface of CdS shell resulting in current flow even at low voltages. For comparison we also performed *I-V* measurement with pristine ZnO nanowires. In this case we observed a noticeable current response only under UV illumination, which is consistent with the band gap energy of ZnO.

* Unpublished results, Manuscript under preparation, 2012.

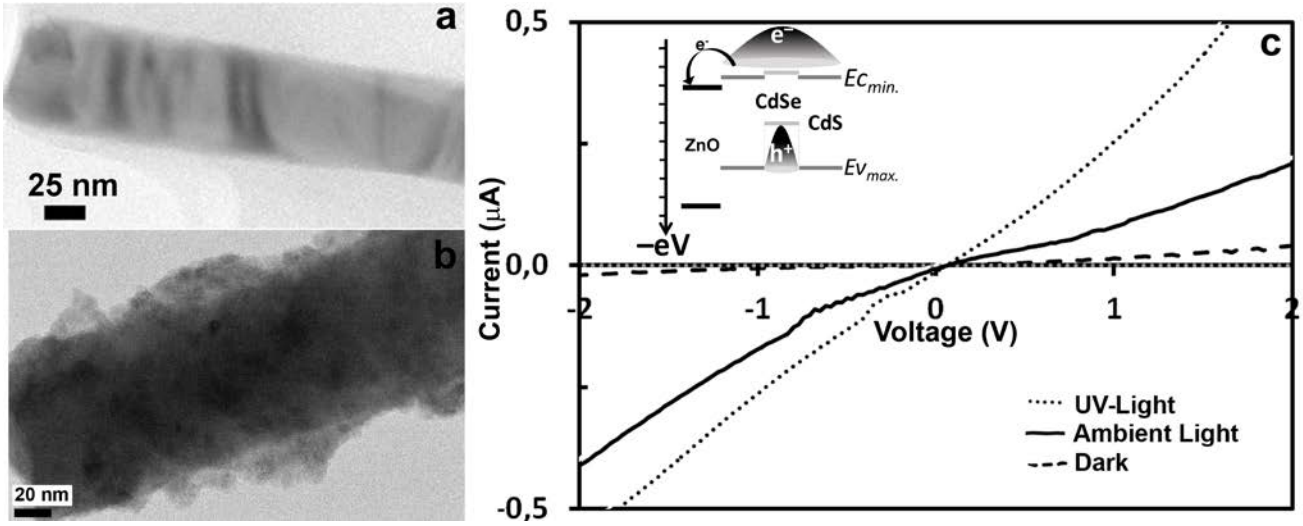

Figure 22. (a) TEM image of a single ZnO nanowire coated with HQDs; inset, TEM image of an uncoated ZnO nanowire as a comparison; **(b)** schematic potential diagram showing the alignment of the energy levels of the HQD-ZnO nanocomposite; **(c)** Typical I-V response curve of the HQD-ZnO nanocomposite, showing no 'turn-on' behavior.

For both these *I-V* measurements, the potential landscape across core-shell interface here is more significant than the exact morphology of the shell. Nevertheless the sharp tips of a tetrahedron may act as concentrators of electric field, and may enhance charge injection into the acceptor materials. It is noteworthy that our results are contrasting to few recent reports, which suggested that electrons are trapped within the central core region for CdSe-CdS HQDs.[160,161]

4. Summary and Conclusions

In this work we have studied different syntheses based on solution chemistry to obtain nanomaterials of II-VI semiconductors, namely ZnO and CdE (E=Te,Se,S), with various anisotropic morphologies. Although the chemical pathways for the syntheses are different, the anisotropic growth has common phenomenological origin, which is based on the anisotropic crystal growth habits of the wurtzite or zinc blende phase (hexagonal and cubic crystal structure, respectively).

We have studied the synthesis of vertically aligned ZnO nanowire arrays, by a chemical bath process on various substrates. The synthesis involves epitaxial growth of ZnO seed-layer on a substrate in a chemical bath containing an aqueous solution of zinc nitrate and hexamine. We have also extended this synthesis to obtain hierarchical nanostructure, which consists of flexible polymeric nanofibers of poly-L-lactide (PLLA) acting as a substrate for the radially oriented growth of ZnO nanowires. We find that this hierarchical PLLA-ZnO nanostructure has a good potential for applications of ZnO pertaining to water purification by photocatalytic reactions occurring at the surface of ZnO. The combination of high surface area and flexibility of the nanofibrous 'substrate' with the photocatalytic functionality of ZnO nanowires enabled the proof-of-principle demonstration of a 'continuous-flow' water treatment system that could effectively degrade single and combination of known organic pollutants in water, as well as render common waterborne bacteria non-viable. Our hierarchical PLLA-ZnO nanostructures can be easily scaled up and the whole photocatalytic water treatment set up can easily be adapted either as a point-of-use system or centralized large-scale water purification system.

We have studied another class of reaction that is commonly used for size controlled synthesis of colloidal quantum dots, which can be modified to obtain anisotropic nanocrystals mainly for CdE (E=S, Se, Te). The mechanism of formation of anisotropic nanocrystals is very similar to the synthesis of ZnO nanowires, wherein the inherently anisotropic crystal growth habit of the wurtzite phase results in rod-shaped or tetrapodal nanocrystals. Since both cubic and hexagonal phases are known for CdE it is possible to manipulate the morphology of the nanocrystal. Anisotropic growth and the morphology of the final nanocrystals depend on the crystal phase of the nuclei. For example, in this thesis we have described synthesis of spherical CdSe quantum dots, tetrapodal CdTe nanocrystals, and tetrahedral core-shell CdSe-CdS nanocrystals. In this work we find that by choosing oleic acid (instead of alkylphosphonic acids) it is possible to synthesize CdTe and CdSe nanotetrapods at much lower temperatures (~180 ºC) than what is commonly reported in the literature and the formation mechanism

is significantly different in our low-temperature reaction compared to the traditional understanding. We have also investigated the feasibility and advantages of microwave mediated synthesis of CdE quatum dots and find that it is both efficient and faster process. The microwave radiation is mainly absorbed by the TOP-E which initiates the decomposition reaction.

The preliminary photoconduction measurements with CdTe nanotetrapods using gold ‘nanogap’ electrodes fabricated in-house, and showed up to 100 times enhancement in current levels in the *I*–*V* measurements under illumination with a white light source. We have also investigated the spatial spread of the excitons in core-shell type-II quantum dots by combining them with an electron acceptor and hole acceptor material. We found from *I*-*V* measurements that the electrons are freely accessible on the surface of the coer-shell quantum dots while the holes encounter a potential barrier, suggesting that the holes are trapped in the core. We also confirmed the spatial localization of the charge carriers in these quantum dots by optical measurements.

5. Future work

A possible topic of future study would be introduction of additional functionalities in the water purification system that would remove heavy metals dissolved in water. The possibility of doped ZnO nanostructrues for photocatalysis of organic pollutants with visible light or sunlight can significantly improve the potential impact of this application. In combination with such functionalities, the water treatment mechanism developed in this work can become truly multifunctional and complete, addressing all major pollutants in water.

The core-shell quasi-type II quantum dots developed in this work have one of the charge carriers trapped within the core, making it difficult to extract without applying a bias voltage. However, the inversing the materials of core and shell, the holes will be trapped in the shell while the electrons will be delocalized throughout the entire nanocrystal. Such quantum dots will retain the non-overlapping electrons and holes wavefunction, thereby reducing the probability of carrier recombination. While at the same time both the charge carriers will be accessible at the surface of the quantum dot. Synthesizing such a quantum dot will be an important future work.

Furthermore, we have investigated separately electron conduction pathways and hole conduction pathways. The next logical step is to combine them to form a single device with the core-shell quantum dots sandwiched between dedicated electron conductors and hole conductors. Such a configuration shows good potential for an efficient photovoltaic device. This should be investigated in the future.

Acknowledgement

I would like to thank my principle supervisor, Assoc. Prof. Muhammet Toprak for his valuable guidance and patience without which much of this work would not have been possible. The resourcefulness and general leadership of my supervisor Prof. Mamoun Muhammed was also valuable for this work. The collaborations, discussions and guidance from Prof. Klaus Leifer, and the group are also gratefully acknowledged. Thanks are also due to Prof. J. Dutta who was my guide and supervisor during the initial stages of my scientific career and his 'never-say-die' style of solving problems will always remain an inspiration for me.

Thanks are also due to several members of the Division of Functional Materials whose direct collaboration has been invaluable, namely Dr. Jian Qin, Dr. Shanghua Li, Dr. A. Uheida. I also thank help and support from my former master student, now my colleague and work partner, Ms. Y. Zhao. I would also like to thank the assistance received, direct and indirect, by former M. Sc. students which led to major parts of this work, namely R. Afrasiabi, Kabir, and V. K. Guduru. I sincerely hope that they all have also benefited from the time spent on working in the lab with me, and it was as much an enriching experience for them as it was for me. I wish them all good luck and hope they make a successful PhD thesis soon.

Instructions received from Wubeshet and Hans on using the transmission electron microscope, and also assistance in scanning electron microscopy from Mazhar and Mohsin were very significant and insightful, and are gratefully acknowledged.

I would like to thank the people involved in writing, following up and maintenance of several current E.U. projects, including NanoEar, NexTec, which funded most of my research. The time spent during my research would not have been as smooth without the discussions, chatting, and the general companionship received from all members of the Division of Functional Materials. Many thanks to Andrea, Carmen, Xiaodi, Ma, Sverker, Fei, Robina, Mazhar, Jafri, Mohsin, Mohsen, *et al*. for their invaluable friendship and companionship during this long journey.

I would like to thank my loving wife whose unconditional love and support was my strength and inspiration until end of 2010. Since then my strength and inspiration came from my wife's biggest gift to me (so far), our little girl Trisha. She is a little bundle of cheerfulness and energy that has brightened up many cold, dark, Stockholm-winter mornings for me. Thanks are also due to my parents whose support and encouragement was and still is very valuable to me.

References

1 P. E. Sheehan, C. M. Lieber, *Science* 272, 1158 (**1996**).

2 F. Yu, J. Zhang, D. Yu, J. He, Z. Liu, B. Xu, Y. Tianb, *J. Appl. Phys.* 105, 094303, (**2009**)

3 M. T. Swihert, *Curr. Opin. Colloid Interface Sci.* 8, 127, (**2003**).

4 T. Nozaki, K. Okazaki, *Plasma Process. Polym.* 5, 300 (**2008**).

5 B. A. Joyce, *Rep. Prog. Phys.* 48, 1637 (**1985**).

6 H. Sakaki, *Phys. Stat. Sol. B*, 215, 291, (**1999**).

7 V. Biju, T. Itoh, A. Anas, A. Sujith, M. Ishikawa, *Anal. Bioanal. Chem.* 391, 2496 (**2008**).

8 Y. Xia, Y. Xiong, B. Lim, S. E. Skrabalak, *Angew. Chem. Int. Ed.* 48, 60 (**2009**).

9 E. C. Scher, L. Manna A. P. Alivisatos, *Phil. Trans. R. Soc. Lond. A* 361, 241 (**2003**).

10 J. Park, K. An, Y. Hwang, J.-G. Park, H.-J. Noh, J.-Y. Kim, J.-H. Park, N.-M. Hwang, T. Hyeon, *Nat. Mater.* 3, 891 (**2004**).

11 X. Michalet, F. F. Pinaud, L. A. Bentolila, J. M. Tsay, S. Doose, J. J. Li, G. Sundaresan, A. M. Wu, S. S. Gambhir, S. Weiss, *Science* 307, 538 (**2005**).

12 S. L. T- McGoldrick, M. Bellanger, M. Caussanel, L. Tsetseris, S. T. Pantelides, S. C. Glotzer, R. D. Schrimpf, *Nano Lett.* 9, 3683 (**2009**).

13 V. I. Klimov, A. A. Mikhailovsky, Su Xu, A. Malko, J. A. Hollingsworth, C. A. Leatherdale, H.-J. Eisler, M. G. Bawendi, *Science* 290, 314 (**2000**).

14 E. S. Jang, J.-H. Won, S.-J. Hwang, J.-H. Choy, *Adv. Mater.* 18, 3309 (**2006**).

15 M. H. Huang, S. Mao, H. Feick, H. Yan, Y. Wu, H. Kind, E. Weber, R. Russo, P. Yang, *Science* 292, 1897 (**2001**).

16 L. E. Greene, M. Law, J. Goldberger, F. Kim, J. C. Johnson, Y. Zhang, R. J. Saykally, P. Yang, *Angew. Chem. Int. Ed.* 42, 3031 (**2003**).

17 A. Sugunan, in 'Photochemical and photoelectric applications of II-VI semiconductor nanomaterials', Licentiate Thesis in Materials Chemistry, Stockholm, **2010**.

18 http://scienceworld.wolfram.com/biography/FranklinBenjamin.html: Accessed on 2010-01-29.

19 B.H. Kear, L. E. Cross, J. E. Keem, R. W. Siegel, E Spaepen, K. C. Taylor, E. L. Thomas and K.-N. Tu, Research Opportunities for Materials with Ultrafine Microstructures, National Academy, Washington, DC, **1989**, Vol. NMAB-454.

20 R. W. Siegel, *NanoStruct. Mater.* 4, 121 (**1994**).

21 B. Gilbert, F. Huang, H. Zhang, G. A. Waychunas, J. F. Banfield. *Science* 305,651 (**2004**).

22 Ph. Buffat, J.-P. Bore, *Phys. Ret. A* 13, 2287 (**1976**).

23 L. Brus, *J. Phys. Chem.* 90, 2555 (**1986**).

24 W. Que, *Phys. Rev. B* 45, 11036 (**1992**).

25 T. Hiramoto, H. Majima, M. Saitoh, *Mater. Sci. Eng. B* 101, 24 (**2003**).

26 http://www-opto.e-technik.uni-ulm.de/lehre/cs/index.html: Accessed on 2010-02-19.

27 M. Koike, S. Nagai, S. Yamasaki, Y. Tezen, A. Kojima, S. Iwayama, *Phys. Stat. Sol. A* 188, 9 (**2001**).

28 S. H. M. Jafri, J. Dutta, D. Sweatman, A. B. Sharma, *Appl. Phys. Lett.* 89, 133123 (**2006**).

29 A. K. Geim, K. S. Novoselov, *Nat. Mater.* 6, 183 (**2007**).

30 R. Juhasz, K. Kylmänen, A. Galeckas, J. Linnros, *Mater. Sci. Eng. C* 25, 733 (**2005**).

31 S. Chen, J. G. Bomer, W. G. van der Wiel, E. T. Carlen, A. van den Berg, *ACS Nano* 3, 3485 (**2009**).

32 V. Tuboltsev, J. Räisänen, *Nanotechnol.* 20, 335302 (**2009**).

33 T. Blom, K. Welch, M. Strømme, E. Coronel, K. Leifer, *Nanotechnol.* 18, 285301 (**2007**).

34 Y. Xia, P. Yang, Y. Sun, Y. Wu, B. Mayers, B. Gates, Y. Yin, F. Kim, H. Yan, *Adv. Mater.* 15, 353 (**2003**).

35 Y. Sun, R. A. Graff, M. S. Strano, J. A. Rogers, *Small* 1, 1052 (**2005**).

36 Z. L. Wang, J. Song, *Science* 312, 242 (**2006**).

37 L. Vayssieres, *Adv. Mater.* 15, 464 (**2003**).

38 A. Dong, R. Tang, W. E. Buhro, *J. Am. Chem. Soc.* 129 12254 (**2007**).

39 Z. A. Peng, X. Peng, *J. Am. Chem. Soc*. 123, 1389 (**2001**).

40 C. R. Martin, *Science* 266, 1961 (**1994**).

41 J. Heremans, C. M. Thrush, Y.-M. Lin, S. Cronin, Z. Zhang, M. S. Dresselhaus, J. F. Mansfield, *Phys. Rev. B* 61, 2921 (**2000**).

42 J. Qin, J. Nogués, M. Mikhaylova, A. Roig, J. S. Muñoz, M. Muhammed, *Chem. Mater.* 17, 1829 (**2005**).

43 Z. Zhang, J. Y. Ying, M. S. Dresselhaus, *J. Mater. Res.* 13, 1745 (**1998**).

44 L. Trahey, C. R. Becker, A. M. Stacy, *Nano Lett.* 7, 2535 (**2007**).

45 Y. Li, G. W. Meng, L. D. Zhang, F. Phillipp, *Appl. Phys. Lett.* 76, 2011 (**2000**).

46 C. Lofton, W. Sigmund, *Adv. Funct. Mater.* 15, 1197 (**2005**).

47 G. Spoto, A. Torrisi, A. Contino, *Chem. Soc. Rev.* 29, 429 (**2000**).

48 L. B. Hunt, *Gold Bull.* 9, 134 (**1976**).

49 C. L. Brown, G. Bushell, M. W. Whitehouse, D. S. Agrawal, S. G. Tupe, K. M. Paknikar, E. R. T. Tiekink, *Gold Bull.* 40, 245 (**2007**).

50 M. Faraday, *Philos. Trans. R. Soc. London*, 147, 145 (**1857**).

51 B. Poudel, Q. Hao, Y. Ma, Y. Lan, A. Minnich, B. Yu, X. Yan, D. Wang, A. Muto, D. Vashaee, X. Chen, J. Liu, M. S. Dresselhaus, G. Chen, Z. Ren, *Science* 320, 634 (**2008**).

52 M. L. Lee, G. Dezsi, R. Venkatasubramanian, *Thin Solid Films* 518, s76 (**2010**).

53 R. Xie, U. Kolb, J. Li, T. Basche, A. Mews, *J. Am. Chem. Soc.* 127, 7480 (**2005**).

54 C.-Y. Chen, C.-T. Cheng, C.-W. Lai, Y.-H. Hu, P.-T. Chou, Y.-H. Chou, H.-T. Chiu, *Small* 1, 1215 (**2005**).

55 L. A. Thomas, L. Dekker, M. Kallumadil, P. Southern, M. Wilson, S. P. Nair, Q. A. Pankhurst, I. P. Parkin, *J. Mater. Chem.* 19, 6529 (**2009**).

56 R. Sarkar, C. S. Tiwary, P. Kumbhakar, A. K. Mitra, *Phys. B* 404, 3855 (**2009**).

57 D. Grosso, P. A. Sermon, *J. Mater. Chem.* 10, 359 (**2000**).

58 S. Jeon, P. V. Braun, *Chem. Mater.* 15, 1256 (**2003**).

59 Z. A. Peng, X. Peng, *J. Am. Chem. Soc.* 124, 3343 (**2002**).

60 C. B. Murray, D. J. Norris, M. D. Bawendi, *J. Am. Chem. Soc.* 115, 8706 (**1993**).

61 A. P. Alivisatos, *J. Phys. Chem.* 100, 13226 (**1996**).

62 A. Leatherdale, W. -K. Woo, F. V. Mikulec, M. G. Bawendi, *J. Phys. Chem. B* 106, 7619 (**2002**).

63 V. I. Klimov, A. A. Mikhailovsky, S. Xu, A. Malko, J. A. Hollingsworth, C. A. Leatherdale, H. -J. Eisler, M. G. Bawendi, *Science* 290, 314 (**2000**).

64 R. A. M. Hikmet, P. T. K. Chin, D. V. Talapin, H. Weller, *Adv. Mater.* 17, 1436 (**2005**).

65 H. Song, S. Lee, *Nanotechnol.* 18, 255202 (**2007**).

66 W. U. Huynh, J. J. Dittmer, A. P. Alivisatos, *Science* 295, 2425 (**2002**).

67 L. Han, D. Qin, X. Jiang, Y. Liu, L. Wang, J. Chen, Y. Cao, *Nanotechnol.* 17, 4736 (**2006**).

68 L. Manna, E. C. Scher, A. P. Alivisatos, *J. Am. Chem. Soc.* 122, 12700 (**2000**).

69 H. Liu, J. S. Owen, A. P. Alivisatos, *J. Am. Chem. Soc.* 129, 305 (**2007**).

70 B. Sun, E. Marx, N. C. Greenham, *Nano Lett.* 3, 961 (**2003**).

71 H. Liu, A. P. Alivisatos, *Nano Lett.* 4, 2397 (**2004**).

72 H. Yan, R. He, J. Pham, P. Yang, *Adv. Mater.* 15, 402 (**2003**).

73 Y. Dai, Y. Zhang, Q. K. Li, C. W. Nan, *Chem. Phys. Lett.* 358, 83 (**2002**).

74 M. Chen, Y. Xie, J. Lu, Y. Xiong, S. Zhang, Y. Qian, X. Liu, *J. Mater. Chem.* 12, 748 (**2002**).

75 Y. -W. Jun, S. -M. Lee, N. -J. Kang, J. Cheon, *J. Am. Chem. Soc.* 123, 5150 (**2001**).

76 H. Chu, X. Li, G. Chen, W. Zhou, Y. Zhang, Z. Jin, J. Xu, Y. Li, *Cryst. Growth Des.* 5, 1801 (**2005**).

77 L. Manna, D. J. Milliron, A. Meisel, E. C. Scher, A. P. Alivisatos, *Nat. Mater.* 2, 382 (**2003**).

78 Y. Li, H. Zhong, R. Li, Y. Zhou, C. Yang, Y. Li, *Adv. Funct. Mater.* 16, 1705 (**2006**).

79 M. B. Mohamed, D. Tonti, A. L. Salman, M. Chergui, *Chem. Phys. Chem.* 6, 2505 (**2005**).

80 K. T. Yong, Y. Sahoo, M. T. Swihart, P. N. Prasad, *Adv. Mater.* 18, 1978 (**2006**).

81 S. Asokan, K. M. Krueger, V. L. Colvin, M. S. Wong, *Small* 3, 1164 (**2007**).

82 S. D. Bunge, K. M. Krueger, T. J. Boyle, M. A. Rodriguez, T. J. Headley, V. L. Colvin, *J. Mater. Chem.* 13, 1705 (**2003**).

83 W. W. Yu, Y. A. Wang, X. Peng, *Chem. Mater.* 15, 4300 (**2003**).

84 L. Carbone, S. Kudera, E. Carlino, W. J. Parak, C. Giannini, R. Cingolani, L. Manna, *J. Am. Chem. Soc.* 128, 748 (**2006**).

85 W. Nie, J. He, N. Zhao, X. Ji, *Nanotechnol.* 17, 1146 (**2006**).

86 A. L. Washington, and G. F. Strouse, *Chem. Mater.* 21, 2770 (**2009**).

87 C. R. Strauss, and R. W. Trainor, *Aust. J. Chem.* 48, 1665 (**1995**).

88 R. J. Giguere, T. L. Bray, S. M. Duncan, and G. Majetich, *Tetrahedron Lett.* 27, 4945 (**1986**).

89 R. Gedye, F. Smith, K. Westaway, H. Ali, L. Baldisera, L. Laberge, and J. Rousell, *Tetrahedron Lett.* 27, 279 (**1986**).

90 N. Kuhnert, *Angew. Chem. Int. Ed.* 41, 1863 (**2002**).

91 A. P. Alivisatos, *Science* 271, 933(**1996**).

92 M. T. Harrison, S. V. Kershaw, A. L. Rogach, A. Kornowski, A. Eychmüller and H. Weller, *Adv. Mater.* 12, 123 (**2000**).

93 D. Steiner, D. Dorfs, U. Banin, F. D. Sala, L. Manna and O. Millo, *Nano Lett.* 8, 2954 (**2008**).

94 B. Mahler, P. Spinicelli, S. Buil, X. Quelin, J. P. Hermier and B. Dubertret, *Nat. Mater.* 7, 659 (**2008**).

95 L. Carbone, C. Nobile, M. D. Giorgi, F. D. Sala, G. Morello, P. Pompa, M. Hytch, E. Snoeck, A. Fiore, I. R. Franchini, M. Nadasan, A. F. Silvestre, L. Chiodo, S. Kudera, R. Cingolani, R. Krahne, L. Manna, *Nano Lett.* 7, 2942 (**2007**).

96 R. M. Kraus, P. G. Lagoudakis, A. L. Rogach, D. V. Talapin, H. Weller, J. M. Lupton and J. Feldmann, *Phys. Rev. Lett.* 98, 017401 (**2007**).

97 D. V. Talapin, R. Koeppe, S. Götzinger, A. Kornowski, J. M. Lupton, A. L. Rogach, O. Benson, J. Feldmann and H. Weller, *Nano Lett.* 3, 1677 (**2003**).

98 L. Fang, J. Y. Park, Y. Cui, A. P. Alivisatos, J. Shcrier, B. Lee, L. W. Wang and M. Salmeron, *J. Chem. Phys.* 127, 184704 (**2007**).

99 X. Y. Kong,Z. L. Wang, *Appl. Phys. Lett.* 84, 975 (**2004**).

100 L. Vayssieres, K. Keis,S. E. Lindquist, A. Hagfeldt, *J. Phys. Chem. B* 105, 3350 (**2001**).

101 Z. R. Tian, J. A. Voigt, J. Liu, B. Mckenzie, M. J. Mcdermott, *J. Am. Chem. Soc.* 124, 12954 (**2002**).

102 S. -C. Liou, C. -S. Hsiao, S. -Y. Chen, *J. Cryst. Growth* 274, 438 (**2005**).

103 J. H. Lee,I. C. Leu, M. H. Hon, *J. Cryst. Growth* 275, 2069 (**2005**).

104 L. E. Greene, M. Law, D. H. Tan, M. Montano, J. Goldberger, G. Somorjai, P. Yang, *Nano Lett.* 5, 1231 (**2005**).

105 K. Govender, D. S. Boyle, P. B. Kenway, P. O'Brien, *J. Mater. Chem.* 14, 2575 (**2004**).

106 L. Dong, J. Jiao, D. W. Tuggle, J. M. Petty, *Appl. Phys. Lett.* 82, 1096 (**2003**).

107 M. Law, L. E. Greene, J. C. Johnson, R. Saykally, P. Yang, *Nat. Mat.* 4, 455 (**2005**).

108 A. Sugunan, J. Dutta, in *Nanotechnology*, (Eds.:G. Schmid, H. Krugs, R. Waser, H. Fuchs, M. Grätzel, K. Kalynanasundaram, L. Chi), Wiley-VCH, Weinheim, Germany **2008**, Vol. 2, Ch. 4.

109 F. D. Mai, C. C. Chen, J. L. Chen, S. C. Liu, *J. Chromatogr. A* 1189, 355 (**2008**).

110 G. Wang, D. Chen, H. Zhang, J. Z. Zhang, J. Li, *J. Phys. Chem. C* 112, 8850 (**2008**).

111 C. –C Chen, *J. Mol. Catal. A: Chem.* 264, 82 (**2007**).

112 I. Poulios, A. Avranas, E. Rekliti, A. Zouboulis, *J. Chem. Technol. Biotechnol.* 75, 205 (**2000**).

113 M. J. Height, S. E. Pratsinis, O. Mekasuwandumrong, P. Praserthdam, *Appl. Catal. B: Environ.* 63, 305 (**2006**).

114 A. Akyol, H. C. Yatmaz, M. Bayramoblu, *Appl. Catal. B: Environ.* 54, 19 (**2004**).

115 H. Gerischer, A. Heller, *J. Phys. Chem.* 95, 5261 (**1991**).

116 T. Ohno, K. Sarukawa, K. Tokieda, M. Matsumura, *J. Catal.* 203, 82 (**2001**).

117 J. Marto, P. S. Marcos, T. Trindade, J. A. Labrincha, *J. Hazard. Mater.* 163, 36 (**2009**).

118 Y. Wang, X. Li, G. Lu, X. Quan, G. Chen, *J. Phys. Chem. C* 112, 7332 (**2008**).

119 S. Baruah, C. Thanachayanont, J. Dutta, *Sci. Technol. Adv. Mater.* 9, 025009 (**2008**).

120 H. Liu, J. Yang, J. Liang, Y. Huang, C. Tang, *J. Am. Ceram. Soc.* 91, 1287 (**2008**).

121 N. Wang, C. Sun, Y. Zhao, S. Zhou, P. Chen, L. Jiang, *J. Mater. Chem.* 18, 3909 (**2008**).

122 S. Kumar, T. Nann, *J. Mater. Res.* 19, 1990 (**2004**).

123 S. L. T- McGoldrick, M. Bellanger, M. Caussanel, L. Tsetseris, S. T. Pantelides, S. C. Glotzer, R. D. Schrimpf, *Nano Lett.* 9, 3683 (**2009**).

124 R. S. Aga Jr., D. Jowhar, M. Ewan, A. Steigerwald, A. Ueda, Z. Pan, W. E. Collins, R. Mu, *J. Phys.: Condens. Mater.* 20, 385206 (**2008**).

125 J.-H. Kim, H. Kim, K. Cho, S. Kim, *Solid State Commun.* 136, 220 (**2005**).

126 H.- Y. Chen, M. K. F. Lo, G. Yang, H. G. Monbouquette, Y. Yang, *Nat. Nanotechnol.* 3, 543 (**2008**).

127 P. -E. Trudeau, M. Sheldon, V. Altoe, A. P. Alivisatos, *Nano Lett.* 8, 1936 (**2008**).

128 Y. Cui, U. Banin, M. T. Björk, A. P. Alivisatos, *Nano Lett.* 5, 1519 (**2005**).

129 J. S. Steckel, J. P. Zimmer, S. Coe-Sullivan, N. E. Stott, V. Bulovic and M. G. Bawendi, *Angew. Chem. Int. Ed.* 43, 2154 (**2004**).

130 M. A. Hines and P. Guyot-Sionnest, *J. Phys. Chem.* 100, 468 (**1996**).

131 R. Xie, X. Zhong and T. Basche, *Adv. Mater.* 17, 2741 (**2005**).

132 S. A. Ivanov, A. Piryatinski, J. Nanda, S. Tretiak, K. R. Zavadil, W. O. Wallace, D. Werder and V. I. Klimov, *J. Am. Chem. Soc.* 129, 11708 (**2007**).

133 V. I: Klimov, S. A. Ivanov, J. Nanda, M. Achermann, I. Bezel, J. A. Mcguire and A. Piryatinski, *Nature* 447, 441 (**2007**).

134 J. Bang, J. Park, J. H. Lee, N. Won, J. Nam, J. Lim, B. Y. Chang, H. J. Lee, B. Chon, J. Shin, J. B. Park, J. H. Choi, K. Cho, S. M. Park, T: Joo and S. Kim, *Chem. Mater.* 22, 233 (**2010**).

135 X. Peng, M. C. Schlamp, A. V. Kadavanich and A. P. Alivisatos, *J. Am. Chem. Soc.* 119, 7019 (**1997**).

136 S. Kim, B. Fisher, H. J. Eisler and M. Bawendi, *J. Am. Chem. Soc.*125, 11466 (**2003**).

137 M. Saba, S. Minniberger, F. Quochi, J. Roither, M. Marceddu, A. Gocalinska, M. V. Kovalenko, D. V. Talapin, W. Heiss, A. Mura and G. Bongiovanni, *Adv. Mater.* 21, 4942 (**2009**).

138 F. Garcia-Santamaria, Y. Chen, J. Vela, R. D. Schaller, J. A. Hollingsworth and V. I. Klimov, *Nano Lett.* 9, 3482 (**2009**).

139 D. V. Talapin, J. H. Nelson, E. V. Shevchenko, S. Aloni, B. Sadtler and A. P. Alivisatos, *Nano Lett.* 7, 2951 (**2007**).

140 D. W. Bahnemann, C. Kormann,R. Hofmann, J. Phys. Chem. 91, 3789 (1987).

141 B. Meyer, D. Marx, *Phys. Rev. B* 67, 035403 (**2003**).

142 Z. R. Tian, J. A. Voigt, J. Liu, B. Mckenzie, M. J. Mcdermott, M. A. Rodriguez, H. Konishi, H. Xu, *Nat. Mater.* 2, 821 (**2003**).

143 H. -L. Liu, T. C.-K. Yang, *Process Biochem.* 39, 475 (**2003**).

144 O. Seven, B. Dindar, S. Aydemir, D. Metin, M. A. Ozinel, S. Icli, *J. Photochem. Photobiol. A* 165, 103 (**2004**).

145 T. Sugimoto, *Adv. Colloid Interface Sci.* 28, 65 (**1987**).

146 J. Y. Rempel, M.G. Bawendi and K.F. Jensen, *J. Am. Chem. Soc.* 131, 4479 (**2009**).

147 W. W. Yu, L. Qu, W. Guo, and X. Peng, *Chem. Mater.* 15, 2854 (**2003**).

148 J. Jasieniak, L. Smith, J. van Embden, P. Mulvaney, *J. Phys. Chem. C* 113, 19468 (**2009**).

149 A. L. Washington, and G. F. Strouse, *J. Am. Chem. Soc.* 130, 8916 (**2008**).

150 Y. Yang, J. Shi, H. Chen, S. Dai and W. Huang, *J. Mater. Res.*17, 2802 (**2002**).

151 Y. V. Klevkov, S. A. Kolosov, A. F. Plotnikov, *Semiconductors* 41, 651 (**2007**).

152 Z. Hu, M. D. Fischbein, C. Querner, M. Drndi, *Nano Lett.* 6, 2585 (**2006**).

153 A. Nemchinov, M. Kirsanova, N. N. Hewa-Kasakarage, M. Zamkov, *J. Phys. Chem. C* 112, 9301 (**2008**).

154 B. D. Boer and A. Facchetti, *Polym. Rev.* 48, 423 (**2008**).

155 S. H. Choi, H. Song, I. K. Park, J. H. Yum, S. S. Kim, S. Lee, and Y. E. Sung, *J. Photochem. Photobiol A* 179, 135 (**2006**).

156 A. Zen, M. Saphiannikova, D. Neher, U. Asawapirom, and U. Scherf, *Chem. Mater.* 17, 781 (**2005**).

157 J.-Y. Chen, C.-C. Kuo, C.-S. Lai, W.-C. Chen, and H.-L. Chen, *Macromolecules* 44, 2883 (**2011**).

158 M. He, J. Ge, M. Fang, F. Qiu, and Y. Yang, *Polymer* 51, 2236 (**2010**).

159 J. Xu, J. Hu, X. Liu, X. Qiu, and Z. Wei, *Macromol. Rapid Commun.* 30, 1419 (**2009**).

160 Z. Ning, H. Tian, H. Qin, Q. Zhang, H. Ågren, L. Sun and Y. Fu, *J. Phys. Chem. C* 114, 15184 (**2010**).

161 D. Steiner, D. Dorfs, U. Banin, F. Della Sala, L. Manna, and O. Millo, *Nano Lett.* 8, 2954 (**2008**)